

This is a repository copy of  *$\beta$  decay of the ground state and of a low-lying isomer in  $^{216}\text{Bi}$* .

White Rose Research Online URL for this paper:

<https://eprints.whiterose.ac.uk/214030/>

Version: Published Version

---

**Article:**

Andel, B., Andreyev, A. N. [orcid.org/0000-0003-2828-0262](https://orcid.org/0000-0003-2828-0262), Blazhev, A. et al. (56 more authors) (2024)  $\beta$  decay of the ground state and of a low-lying isomer in  $^{216}\text{Bi}$ . Phys. Rev. C. 064321. ISSN 2469-9993

<https://doi.org/10.1103/PhysRevC.109.064321>

---

**Reuse**

This article is distributed under the terms of the Creative Commons Attribution (CC BY) licence. This licence allows you to distribute, remix, tweak, and build upon the work, even commercially, as long as you credit the authors for the original work. More information and the full terms of the licence here:

<https://creativecommons.org/licenses/>

**Takedown**

If you consider content in White Rose Research Online to be in breach of UK law, please notify us by emailing [eprints@whiterose.ac.uk](mailto:eprints@whiterose.ac.uk) including the URL of the record and the reason for the withdrawal request.

**$\beta$  decay of the ground state and of a low-lying isomer in  $^{216}\text{Bi}$** 

B. Andel<sup>1,\*</sup>, A. N. Andreyev<sup>2,3</sup>, A. Blazhev<sup>4</sup>, R. Ličá<sup>5</sup>, H. Naïdja<sup>6</sup>, M. Stryjczyk<sup>7,8</sup>, P. Van Duppen<sup>7</sup>, A. Algora<sup>9,10</sup>, S. Antalic<sup>1</sup>, A. Barzakh<sup>11</sup>, J. Benito<sup>12</sup>, G. Benzoni<sup>13</sup>, T. Berry<sup>14</sup>, M. J. G. Borge<sup>15</sup>, K. Chrysalidis<sup>16</sup>, C. Clisu<sup>5</sup>, C. Costache<sup>5</sup>, J. G. Cubiss<sup>2</sup>, H. De Witte<sup>7</sup>, D. V. Fedorov<sup>11</sup>, V. N. Fedosseev<sup>16</sup>, L. M. Fraile<sup>12</sup>, H. O. U. Fynbo<sup>17</sup>, P. T. Greenlees<sup>8</sup>, L. J. Harkness-Brennan<sup>18</sup>, M. Huyse<sup>7</sup>, A. Illana<sup>19</sup>, J. Jolie<sup>4</sup>, D. S. Judson<sup>18</sup>, J. Konki<sup>8</sup>, I. Lazarus<sup>20</sup>, M. Madurga<sup>16</sup>, N. Marginean<sup>5</sup>, R. Marginean<sup>5</sup>, B. A. Marsh<sup>16,†</sup>, C. Mihai<sup>5</sup>, P. L. Molkanov<sup>11</sup>, P. Mosat<sup>1</sup>, J. R. Murias<sup>12,21</sup>, E. Nacher<sup>9</sup>, A. Negret<sup>5</sup>, R. D. Page<sup>18</sup>, S. Pascu<sup>5</sup>, A. Perea<sup>15</sup>, V. Pucknell<sup>20</sup>, P. Rahkila<sup>8</sup>, E. Rapisarda<sup>16</sup>, K. Rezyunkina<sup>7,22</sup>, V. Sánchez-Tembleque<sup>12</sup>, K. Schomacker<sup>4</sup>, M. D. Seliverstov<sup>11</sup>, C. Sotty<sup>5</sup>, L. Stan<sup>5</sup>, C. Sürder<sup>23</sup>, O. Tengblad<sup>15</sup>, V. Vedia<sup>12</sup>, S. Viñals<sup>15</sup>, R. Wadsworth<sup>2</sup>, and N. Warr<sup>4</sup>

(IDS Collaboration)

<sup>1</sup>Department of Nuclear Physics and Biophysics, Comenius University in Bratislava, 84248 Bratislava, Slovakia<sup>2</sup>School of Physics, Engineering and Technology, York YO10 5DD, United Kingdom<sup>3</sup>Advanced Science Research Center, Japan Atomic Energy Agency, Tokai-mura, Ibaraki 319-1195, Japan<sup>4</sup>Institut für Kernphysik, Universität zu Köln, 50937 Köln, Germany<sup>5</sup>“Horia Hulubei” National Institute for R & D in Physics and Nuclear Engineering, RO-077125 Bucharest, Romania<sup>6</sup>Laboratoire de Physique Mathématique et Physique Subatomique, Université Constantine 1, Constantine 25000, Algeria<sup>7</sup>KU Leuven, Instituut voor Kern- en Stralingsfysica, B-3001 Leuven, Belgium<sup>8</sup>University of Jyväskylä, Department of Physics, Accelerator laboratory, P.O. Box 35(YFL) FI-40014 University of Jyväskylä, Finland<sup>9</sup>Instituto de Física Corpuscular, CSIC - Universidad de Valencia, E-46980 Valencia, Spain<sup>10</sup>Institute of Nuclear Research (ATOMKI), P.O.Box 51, H-4001 Debrecen, Hungary<sup>11</sup>Affiliated with an institute covered by a cooperation agreement with CERN<sup>12</sup>Grupo de Física Nuclear, Universidad Complutense de Madrid, 28040, Madrid, Spain<sup>13</sup>Istituto Nazionale di Fisica Nucleare, Sezione di Milano, I-20133 Milano, Italy<sup>14</sup>Department of Physics, University of Surrey, Guildford GU2 7XH, United Kingdom<sup>15</sup>Instituto de Estructura de la Materia, CSIC, Serrano 113 bis, E-28006 Madrid, Spain<sup>16</sup>CERN, CH-1211 Geneve 23, Switzerland<sup>17</sup>Department of Physics and Astronomy, Aarhus University, DK-8000 Aarhus C, Denmark<sup>18</sup>Department of Physics, Oliver Lodge Laboratory, University of Liverpool, Liverpool L69 7ZE, United Kingdom<sup>19</sup>Instituto Nazionale di Fisica Nucleare, Laboratori Nazionali di Legnaro, I-35020 Legnaro, Italy<sup>20</sup>STFC Daresbury, Daresbury, Warrington WA4 4AD, United Kingdom<sup>21</sup>Institut Laue-Langevin, CS 20156, 38042 Grenoble Cedex 9, France<sup>22</sup>Université de Strasbourg, CNRS, IPHC UMR7178, F-67000, Strasbourg, France<sup>23</sup>Institut für Kernphysik, Technische Universität Darmstadt, 64289 Darmstadt, Germany

(Received 24 January 2024; accepted 26 April 2024; published 24 June 2024)

A detailed  $\beta$ -decay study of the low- and high-spin states in  $^{216}\text{Bi}$  has been performed at the ISOLDE Decay Station at the CERN-ISOLDE facility. In total, 48 new levels and 83 new transitions in the  $\beta$ -decay daughter  $^{216}\text{Po}$  were identified. Shell-model calculations for excited states in  $^{216}\text{Bi}$  and  $^{216}\text{Po}$  were performed using the H208 and the modified Kuo-Herling particle effective interactions. Based on the experimental observations and the shell-model calculations, the most likely spin and parity assignments for the  $\beta$ -decaying states in  $^{216}\text{Bi}$  are  $(3^-)$  and  $(8^-)$ , respectively.

DOI: [10.1103/PhysRevC.109.064321](https://doi.org/10.1103/PhysRevC.109.064321)**I. INTRODUCTION**

The neutron-rich odd-odd bismuth isotopes ( $Z = 83$ ) with one proton above the closed shell at  $Z = 82$  and a few neutrons above the closed shell at  $N = 126$  provide an

\*boris.andel@fmph.uniba.sk

†Deceased.

exceptional tool for testing shell-model (SM) calculations. The ground state (g.s.) and the lowest-lying excited states stem dominantly from the  $[\pi 0h_{9/2} \otimes \nu(1g_{9/2})^n]_{0^-, \dots, 9^-}$   $p$ - $n$  multiplet and their ordering may result in the presence of low-lying  $\beta$ -decaying isomers, as observed in, e.g.,  $^{210,212}\text{Bi}$  [1,2]. In our recent study, a low-lying ( $8^-$ ) isomer was identified also in  $^{214}\text{Bi}$  and its  $\beta$  decay to the excited states in  $^{214}\text{Po}$  was investigated [3]. Two or possibly three  $\beta$ -decaying states were proposed also in  $^{216}\text{Bi}$  in earlier works [4,5], as discussed further in this section.

The present study aims at the detailed spectroscopic investigation of the  $\beta^-$  decay of  $^{216}\text{Bi}$  to excited states in  $^{216}\text{Po}$ . It is a part of our systematic study of the bismuth isotopic chain including (i) laser-spectroscopy measurements yielding mean-squared charge radii and magnetic moments [6], and (ii) investigation of the underlying structure of the yrast states in  $^{214,216,218}\text{Po}$  (populated in  $\beta^-$  decay of  $^{214,216,218}\text{Bi}$ ) via lifetime measurements, which provide transition strengths [7]. The recent  $\beta$ -decay study of  $^{214}\text{Bi}$  [3] and the present investigation of  $^{216}\text{Bi}$  were performed during the latter experiment. As a first step, the level structure and decay paths in the daughter polonium isotopes need to be understood. For example, the  $^{214}\text{Bi}$  study revealed two new levels with strong  $\beta$ -decay feeding, one of them only 49 keV above the  $8_1^+$  state in  $^{214}\text{Po}$  [3]. This new information will play a role in the analysis of the mentioned lifetime measurements.

The  $^{216}\text{Bi}$  ( $N = 133$ ) isotope was observed for the first time at ISOLDE (CERN), as an  $\alpha$ -decay product of  $^{220}\text{At}$  [8]. A half-life of 6.6(21) min. was reported, but no details on its determination were provided. In a later study at the Institut de Physique Nucléaire d'Orsay [9],  $^{216}\text{Bi}$  was produced in a spallation reaction in  $^{232}\text{Th}$  target induced by 200-MeV proton beam. A  $\beta^-$  decay of  $^{216}\text{Bi}$  to 550-keV ( $2^+$ ) and 969-keV ( $4^+$ ) [spin unknown at the time] levels in  $^{216}\text{Po}$  was identified and a shorter half-life of 3.6(4) min. was determined. Roughly equally strong  $\beta$ -decay feeding to these two levels hinted at a low spin of the initial state in  $^{216}\text{Bi}$  [9].

In the second  $\beta$ -decay experiment performed at ISOLDE using 1-GeV proton beam and  $^{232}\text{Th}$  target, the population of the yrast band in  $^{216}\text{Po}$ , up to the ( $8^+$ ) level, and of several states above it, up to 2.2 MeV, was observed [4]. The feeding pattern suggested a high spin for the  $\beta$ -decaying state in  $^{216}\text{Bi}$ . In addition, a half-life of 135(5) s was deduced. These observations were in contradiction to the previous studies [8,9]. To explain discrepancies in the observed feeding and determined half-life values between different measurements, the presence of two  $\beta$ -decaying states in  $^{216}\text{Bi}$ , one with a low spin and one with a high spin, was suggested [4], while different contributions of each state would have been present in respective measurements. The high-spin state was proposed to be the g.s. with  $I^\pi = (6^-, 7^-)$ , but the strong feeding to the ( $8^+$ ) level in  $^{216}\text{Po}$ , possibly hinting a spin up to ( $9^-$ ) for the  $\beta$ -decaying state in  $^{216}\text{Bi}$ , was also discussed [4].

The most recent  $\beta$ -decay study of  $^{216}\text{Bi}$ , performed at the GSI, employed a fragmentation reaction of a 1-GeV  $^{238}\text{U}$  beam on a beryllium target [5]. The  $^{216}\text{Bi}$  isotope was produced both directly and via  $\beta^-$  decay of  $^{216}\text{Pb}$ . The decay scheme of the high-spin state reported in the second ISOLDE

work [4] was confirmed and a similar half-life of 133(15) s was deduced. Moreover, several new levels deexciting to the yrast ( $4^+$ ) and  $2^+$  states in  $^{216}\text{Po}$  were identified. It was argued that, since these new states were not observed in Ref. [4], where  $^{216}\text{Bi}$  was produced directly, they arise from the  $\beta^-$  decay of a low-spin, possibly a new  $I = (0, 1)$  isomer in  $^{216}\text{Bi}$  produced indirectly via  $\beta^-$  decay of the  $0^+$  g.s. in  $^{216}\text{Pb}$ . A half-life was not measured for this low-spin isomer [5].

In the most up-to-date NUBASE 2020 evaluation [10], the low-spin state in  $^{216}\text{Bi}$  is tentatively assigned as an  $I^\pi = (3^-)$  isomer with an excitation energy of 24(19) keV. The procedure [11] to deduce this excitation energy used the  $Q_\alpha$  value for  $^{220}\text{At}$  [8], and the atomic masses of the  $^{220}\text{At}$  g.s. [12] and the  $^{216}\text{Bi}$  g.s. [13]. The tentative spin of (3) was also suggested in the Evaluated Nuclear Structure Data File (ENSDF) [14] based on the population of this state in the unhindered  $\alpha$  decay of the g.s. of  $^{220}\text{At}$  ( $I = 3$ ).

In the present work, feeding of both low-spin and high-spin states in  $^{216}\text{Po}$  was observed and many new levels and transitions were identified. It allows us to shed more light on the uncertain properties of  $^{216}\text{Bi}$   $\beta^-$  decay and provides detailed information on excited states in  $^{216}\text{Po}$ . Because of the large uncertainty of the isomer excitation energy of 24(19) keV [10], the order of the states in  $^{216}\text{Bi}$  is not firmly established, but for simplicity and consistency with the literature [4,5,10,14], the high-spin state will be further on referred to as  $^{216}\text{Bi}^g$ . Although Ref. [5] raised the possibility of the presence of two low-spin isomers in  $^{216}\text{Bi}$ , our data do not confirm this suggestion. Therefore, the state feeding low-spin levels in  $^{216}\text{Po}$  will be referred to as  $^{216}\text{Bi}^m$ . The issue will be addressed in more detail in Sec. IV C.

## II. EXPERIMENT

The  $^{216}\text{Bi}$  isotope was measured in the same experimental campaign as described for  $^{214}\text{Bi}$  in Ref. [3]. The nuclei of interest were produced at the ISOLDE facility at CERN [16,17] in proton-induced spallation reactions in a thick  $\text{UC}_x$  target (50 g/cm<sup>2</sup>). A pulsed beam of 1.4-GeV protons was provided by the Proton Synchrotron Booster. The proton pulses were grouped into a so-called supercycle, containing typically around 30 pulses, part of which was delivered to the ISOLDE target. An average beam intensity was up to 2  $\mu\text{A}$ .

The produced isotopes diffused through the target material heated to  $\approx 2300$  K and effused into a hot cavity, where they were subsequently ionized by the Resonance Ionization Laser Ion Source (RILIS) [18,19]. A three-step resonance ionization scheme using laser light with wavelengths of 306.9, 555.4, and 532 nm (the third being nonresonant) [20] was employed to selectively ionize bismuth isotopes. The frequency of the first-step laser was set to a specific hyperfine transition for  $^{216}\text{Bi}^g$ . However, the hyperfine components of  $^{216}\text{Bi}^{g,m}$  partially overlap and a broad linewidth of the laser of  $\approx 12$  GHz was employed, therefore both  $^{216}\text{Bi}^g$  and  $^{216}\text{Bi}^m$  were ionized at the same time. The ions were extracted and accelerated by a 50 kV potential. Then they were mass-separated by the high resolution separator according to their mass-to-charge ratio  $A/q = 216$ .

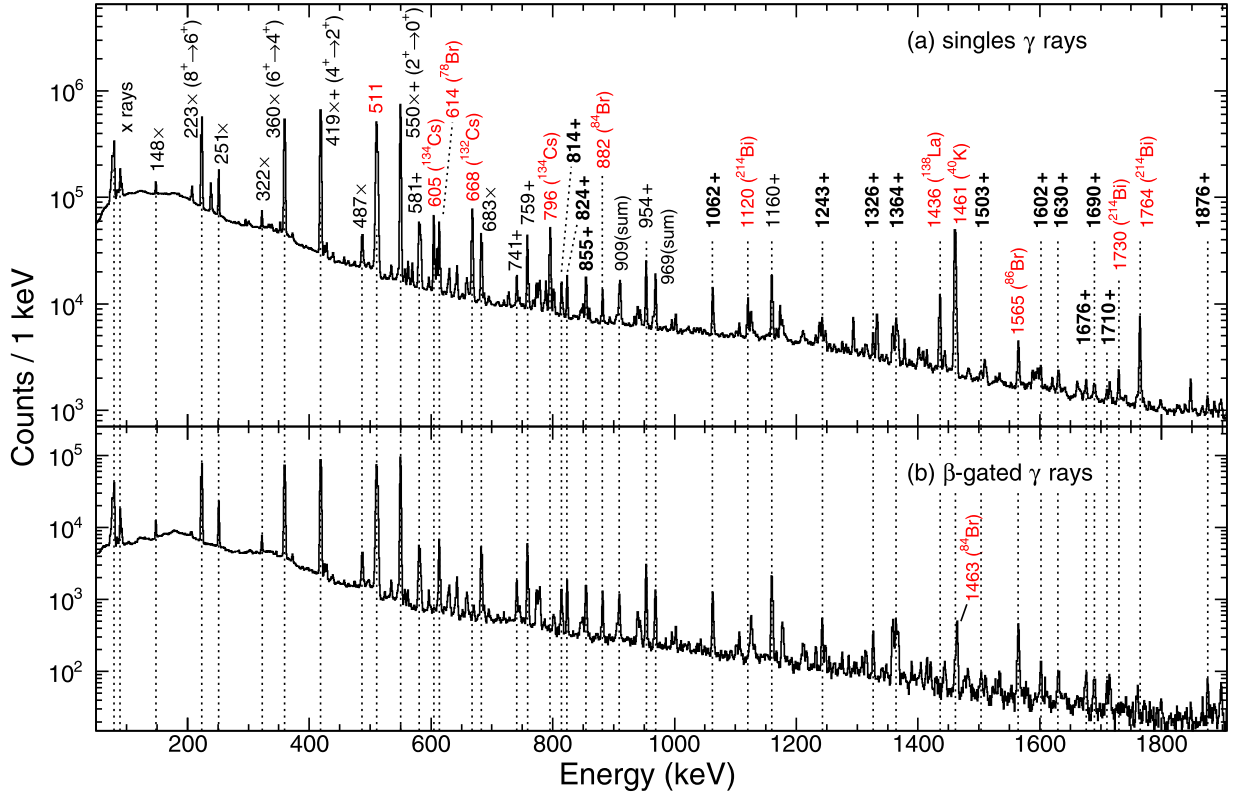


FIG. 1. A part of (a) the singles  $\gamma$ -ray spectrum and (b) the  $\beta$ -gated  $\gamma$ -ray spectrum. The peaks marked with (x) and (+) labels follow the  $\beta^-$  decays of  $^{216}\text{Bi}^g$  and  $^{216}\text{Bi}^m$ , respectively. The labels written in bold denote new transitions. Peaks marked with “(sum)” originate from the summing of transitions in cascades; they are listed in Table II in the Supplemental Material [15]. The remaining peaks highlighted in red belong to background or contamination in the beam. In cases where the peak is a doublet, only the energy of the dominant transition is stated.

The mass-separated ion beam was delivered to the ISOLDE Decay Station (IDS) [21] and implanted on an aluminized Mylar<sup>®</sup> tape. Four HPGe clover detectors for  $\gamma$ -ray detection were placed outside the vacuum chamber in close geometry around the implantation position. A plastic scintillator for  $\beta$ -particle detection was mounted behind a thin plastic window of the vacuum chamber at the implantation point. The detection efficiency of  $\beta$  particles feeding the levels in  $^{216}\text{Po}$  at around 2 MeV, for which  $\beta$  electron energy distribution ends at  $E_{\beta, \text{max}} = Q_{\beta} - E_{\text{level}} \approx 2$  MeV, was  $\approx 14\%$ . The detection system also included two  $\text{LaBr}_3(\text{Ce})$  detectors for lifetime measurements of excited states [7], which will be reported elsewhere [22].

The energy calibration of the HPGe detectors was performed with a  $^{152}\text{Eu}$  source. The energy resolution for the 223- and 1160-keV  $\gamma$  rays following the  $\beta^-$  decay of  $^{216}\text{Bi}$  was 2.0 and 2.5 keV (full width at half maximum, FWHM), respectively. The uncertainty of the energy calibration is estimated to be below 0.2 keV for energies up to  $\approx 2.5$  MeV and around 0.3 keV for energies up to  $\approx 3$  MeV based on the comparison with the known  $\gamma$ -ray peaks in our data coming from natural background and contamination in the beam, see Table I and Fig. 1 in the Supplemental Material [15] (including Refs. [23–32]). For the absolute detection efficiency calibration, intensity-calibrated sources of  $^{152}\text{Eu}$  and  $^{133}\text{Ba}$  were used. The absolute detection efficiency

at 223 and 1160 keV was 10.7(3)% and 4.1(1)%, respectively.

All  $\gamma$ -ray spectra were created using add-back for all four crystals within each clover detector. Background subtraction for  $\gamma$ - $\gamma$  coincidence spectra and for time distribution spectra was done by gating on the background on the left-hand side and on the right-hand side of the peak of interest. Extracted  $\gamma$ -ray intensities were corrected for summing of  $\gamma$  rays in cascades.

### III. RESULTS

#### A. Introduction to the data analysis

Parts of the singles  $\gamma$ -ray and  $\beta$ -gated  $\gamma$ -ray spectra are shown in Figs. 1(a) and 1(b), respectively. The  $\beta$ - $\gamma$  coincidence time window was  $|\Delta t(\beta\text{-}\gamma)| < 200$  ns. Most of the dominant peaks in Fig. 1(a) below 700 keV are the known transitions following the  $\beta^-$  decay of  $^{216}\text{Bi}^g$ , such as the 223.3- ( $8^+ \rightarrow 6^+$ ), 359.6- ( $6^+ \rightarrow 4^+$ ), 418.8- ( $4^+ \rightarrow 2^+$ ) and 549.8-keV  $2^+ \rightarrow 0^+$  yrast transitions [4]. Moreover, intense transitions following the  $\beta^-$  decay of  $^{216}\text{Bi}^m$ , identified in Ref. [5], are also seen, for example, at 758.6, 953.5, and 1160.0 keV. Several new transitions attributed to the  $\beta^-$  decay of  $^{216}\text{Bi}^m$  are labeled in bold. The numbers of decayed nuclei for each of the states were deduced as  $N(^{216}\text{Bi}^m) = 1.45(1) \times 10^7$  and  $N(^{216}\text{Bi}^g) = 1.51(1) \times 10^7$ , resulting in the observed

isomer ratio of 0.96(1). Details on the determination of contribution of the respective state are given in Sec. III E.

Apart from the transitions following the  $\beta^-$  decay of  $^{216}\text{Bi}^{g,m}$ ,  $\gamma$  rays originating from the natural background ( $\beta^-$  decay of  $^{214}\text{Bi}^g$ , EC/ $\beta^+$  decay of  $^{40}\text{K}$ ), intrinsic activity of the  $\text{LaBr}_3(\text{Ce})$  detectors (EC/ $\beta^+$  decay of  $^{138}\text{La}$  [33]) and contaminants in the beam are present in Fig. 1. Specifically, transitions following EC/ $\beta^+$  decay of  $^{78}\text{Br}$ ,  $^{132}\text{Cs}$ , and  $\beta^-$  decay of  $^{84}\text{Br}$ ,  $^{86}\text{Br}$ , and  $^{134}\text{Cs}$  were identified. Isotopes of bromine most likely passed through the mass separator in the form of  $\text{BaBr}^+$  molecules with the selected mass [34]. Cesium isotopes are long-lived nuclides, which were deposited in the vicinity of the implantation point in one of the previous measurements. We note that the 614-keV  $\gamma$  ray following the EC/ $\beta^+$  decay of  $^{78}\text{Br}$  is present also in the  $\beta^-$ -gated  $\gamma$ -ray spectrum in Fig. 1(b), because the relevant level is dominantly populated by the  $\beta^+$ -decay branch [24].

To reliably distinguish transitions following the  $\beta^-$  decay of  $^{216}\text{Bi}^{g,m}$  from the contaminants and to build decay schemes,  $\gamma$ - $\gamma$  coincidence analysis was used. It has a sufficient selectivity, thus, an additional  $\beta^-$ -gating was not employed. The prompt coincidence time window was  $|\Delta t(\gamma-\gamma)| < 200$  ns.

Generally, transitions feeding the ( $6^+$ ) or ( $8^+$ ) levels in  $^{216}\text{Po}$ , or feeding the structures on top of these levels, were attributed to the  $\beta^-$  decay of the high-spin  $^{216}\text{Bi}^g$ . The remaining transitions, feeding either directly or via a cascade of  $\gamma$  rays to the ( $4^+$ ),  $2^+$ , or  $0^+$  levels in  $^{216}\text{Po}$ , were attributed to the  $\beta^-$  decay of the low-spin  $^{216}\text{Bi}^m$ . Exceptions are discussed in the sections for  $^{216}\text{Bi}^g$  (Sec. III B) and  $^{216}\text{Bi}^m$  (Sec. III C). Ambiguity in attributing levels decaying only to the ( $4^+$ ) level or to the structure above this state in the decay scheme of  $^{216}\text{Bi}^m$  is discussed in Sec. III C.

Gamma-ray intensities shown in Tables I and II were determined from the singles  $\gamma$  rays, where possible. If the peak was a doublet with one component being dominant, the intensity of the dominant  $\gamma$  ray was corrected for the contribution of the smaller component using  $\gamma$ - $\gamma$  coincidences or using the known  $\gamma$ -ray intensities in the case of contaminants. Intensities for the remaining transitions were determined from  $\gamma$ - $\gamma$  coincidences. In these cases, the intensities may be influenced by angular dependence between  $\gamma$  rays. This effect was estimated by comparing intensities from singles  $\gamma$  rays and from  $\gamma$ - $\gamma$  coincidences for selected intense transitions. Typically, the discrepancies were up to  $\approx 15\%$ , thus an additional systematic uncertainty of 15% was added in quadrature to uncertainties of the intensities extracted from  $\gamma$ - $\gamma$  coincidences.

To calculate the total transition intensities, a correction for internal conversion had to be employed. However, with the exception of the four yrast transitions for which an  $E2$  character is assumed, multipolarities of  $\gamma$ -ray transitions following the  $\beta^-$  decay of  $^{216}\text{Bi}^{g,m}$  are unknown. To estimate the total internal conversion coefficients  $\alpha_{\text{tot}}$ , we used the prompt character of the  $\gamma$  rays to limit their possible multipolarities. The prompt character was confirmed for almost all of the relevant  $\gamma$  rays by their at least tentative presence in the  $\beta^-$ -gated  $\gamma$ -ray spectrum. A comparison of the singles and  $\beta^-$ -gated  $\gamma$  rays is shown for the part of the energy range and selected intense transitions in Figs. 1(a) and 1(b), respectively. The only exceptions were the weak 283.3- and 305.2-keV

transitions hidden in the Compton background (Tables I and II) and the transitions deexciting levels at energies above 3 MeV (Table IV in the Supplemental Material [15]). The latter could not have been confirmed in the  $\beta^-$ -gated spectrum, because of the weak  $\gamma$ -ray intensities and decreasing detection efficiency for  $\beta$  particles with decreasing  $E_{\beta,\text{max}} = Q_{\beta} - E_{\text{level}}$ .

For  $\gamma$ -ray transition energies below 600 keV we considered  $E1$ ,  $M1$ , and  $E2$  multipolarities, while for higher energies  $M2$  and  $E3$  multipolarities were also included. The total internal conversion coefficients  $\alpha_{\text{tot}}$  were estimated as an average of the lowest theoretical value [ $\alpha_{\text{tot,th}}(E1)$ ] and the highest theoretical value [either  $\alpha_{\text{tot,th}}(M1)$  or  $\alpha_{\text{tot,th}}(M2)$ ] taken from Ref. [32]. The uncertainty is the difference between the highest and the lowest value divided by two. Specific values of these  $\alpha_{\text{tot}}$  estimates are listed in Tables III and IV in the Supplemental Material [15]. For the 486.1-keV transition,  $\alpha_{\text{tot,expt}}$  deduced in Sec. III B was used. Numbers of counts for transitions ( $N_t$ ), needed for determination of transition intensities, were then deduced in a usual way as

$$N_t = N_{\gamma}(1 + \alpha_{\text{tot}}), \quad (1)$$

where  $N_{\gamma}$  is the number of counts for a given  $\gamma$ -ray transition corrected for detection efficiency.

## B. $\beta^-$ decay of $^{216}\text{Bi}^g$

The decay scheme of  $^{216}\text{Bi}^g$  from Ref. [4] was confirmed by  $\gamma$ - $\gamma$  coincidences and extended by adding 16 new  $\gamma$ -ray transitions and 12 new levels (Fig. 2 and Table I). Level energies were deduced from  $\gamma$ -ray energies. In the case of parallel decay paths from the specific level, weighted average of the resulting energies was used, excluding paths with tentative transitions, where possible. Coincident  $\gamma$ -ray spectra with transitions depopulating high-spin yrast levels, i.e., the 223.3-keV ( $8^+$ )  $\rightarrow$  ( $6^+$ ) and 359.6-keV ( $6^+$ )  $\rightarrow$  ( $4^+$ ) transitions, are shown in Figs. 3 and 4, respectively. The collected statistics were more than an order of magnitude higher than in the previous study [4]: there are about 2000 counts in the 223.3-keV peak in the spectrum gated on the 359.6-keV transition in Fig. 1 in Ref. [4], while in our study there were  $5.5 \times 10^4$  counts for the same  $\gamma$ - $\gamma$  coincidence shown in Fig. 3(b).

The energies of most  $\gamma$ -ray transitions fit within 0.1 keV with the values from Ref. [4]. Notable exceptions are the 682.8- and 487.3-keV transitions, which were reported with energies of 682.0 and 486.9 keV in Ref. [4], and no uncertainties were given. However, the 682.0-keV value may be a graphical error, because the energy values for this transition given for gates in  $\gamma$ - $\gamma$  coincidences in Ref. [4] are 682.4, 682.6, 682.7, and 682.8 keV. The 487-keV peak in Fig. 1 was in the present work found to be a doublet consisting of the 487.3- and 486.1-keV  $\gamma$  rays, which explains the discrepancy with Ref. [4], where it was considered as a single transition. The dominant contribution is the 487.3-keV  $\gamma$  ray feeding the 1551.5-keV level as reported in Ref. [4]. The energy of 487.3 keV was deduced from the gate on the 223.3-keV transition in  $\gamma$ - $\gamma$  coincidences shown in Fig. 3(a). The energy of the weaker, newly identified 486.1-keV transition was deduced

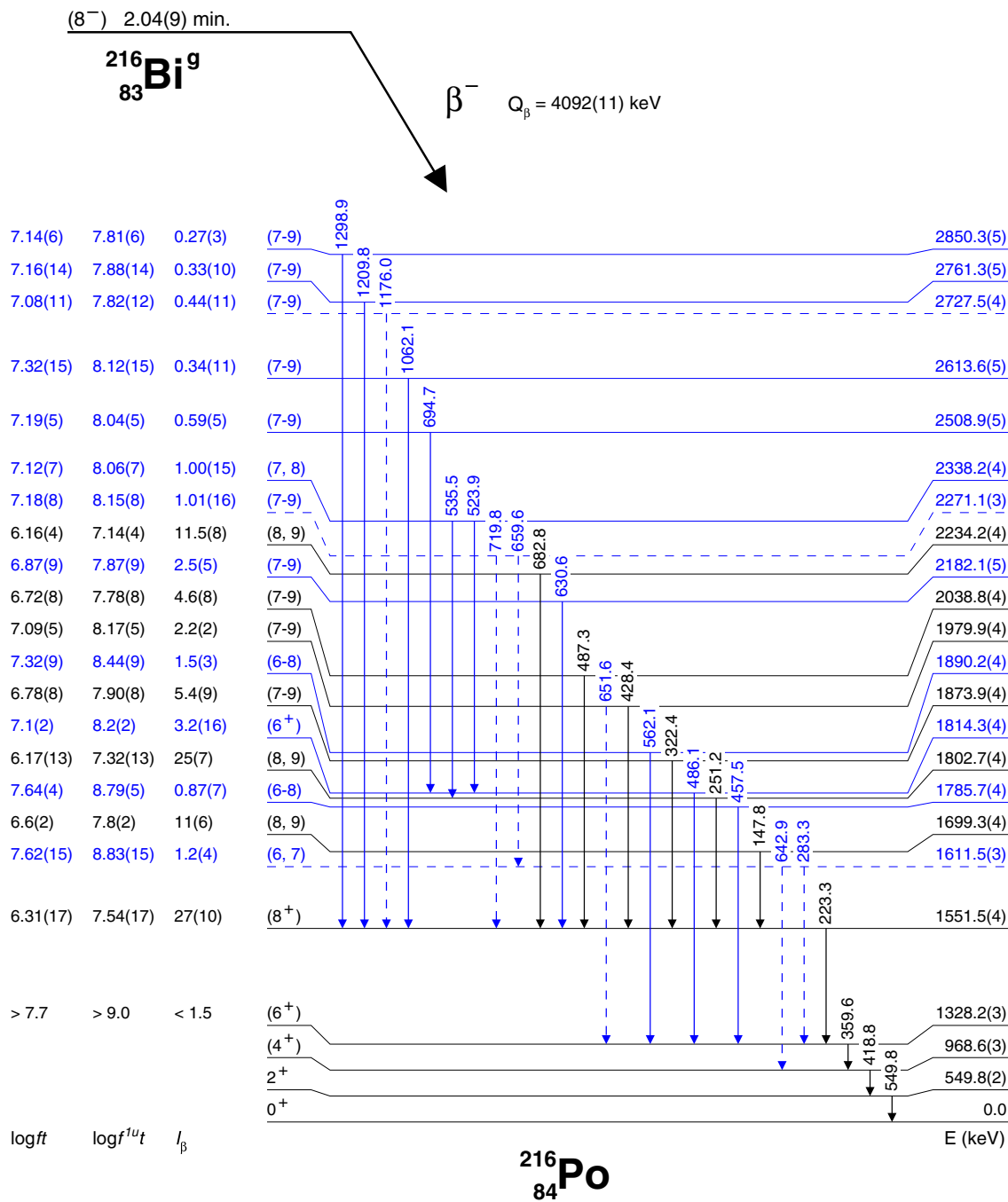


FIG. 2. The decay scheme with levels in <sup>216</sup>Po populated by the β<sup>-</sup> decay of <sup>216</sup>Bi<sup>g</sup>. The new transitions and levels from the present study are highlighted in blue, while those in black font were reported in Refs. [4,5]. The half-life of <sup>216</sup>Bi<sup>g</sup>, β-decay feeding intensities and log(ft), log(f<sup>1u</sup>t) values are from this work. All spin and parity assignments are from this work, with an exception of the yrast levels in <sup>216</sup>Po up to the (8<sup>+</sup>) state, which were taken from Ref. [4]. The Q<sub>β</sub> value was taken from AME 2020 [35]. For display purposes, the levels up to the (6<sup>+</sup>) state are spaced evenly. Dashed lines denote tentatively placed transitions and levels.

using the gate on the 694.7-keV γ ray, see Fig. 2(a) in the Supplemental Material [15]. We note that the 1950-keV level in Ref. [4] is presumably a graphical error and corresponds to the 1979.9-keV level in Fig. 2 based on the energies of deexciting γ-ray cascade.

In Ref. [5], a 304-keV γ ray was suggested to be in coincidence with the 359.6-keV transition. However, we could

not confirm the 304-keV γ ray despite orders-of-magnitude higher statistics. For example, the 359.6-keV peak contained 1.1 × 10<sup>6</sup> counts in γ-ray singles in the present work (Fig. 1), while in the γ-ray spectrum in Fig. 7 in Ref. [5] it contained ≈600 counts. It has to be noted that Fig. 7 in Ref. [5] showed β-gated γ rays tagged on subsequent α decays of the β-decay daughter <sup>216</sup>Po, where the α particle detection efficiency was

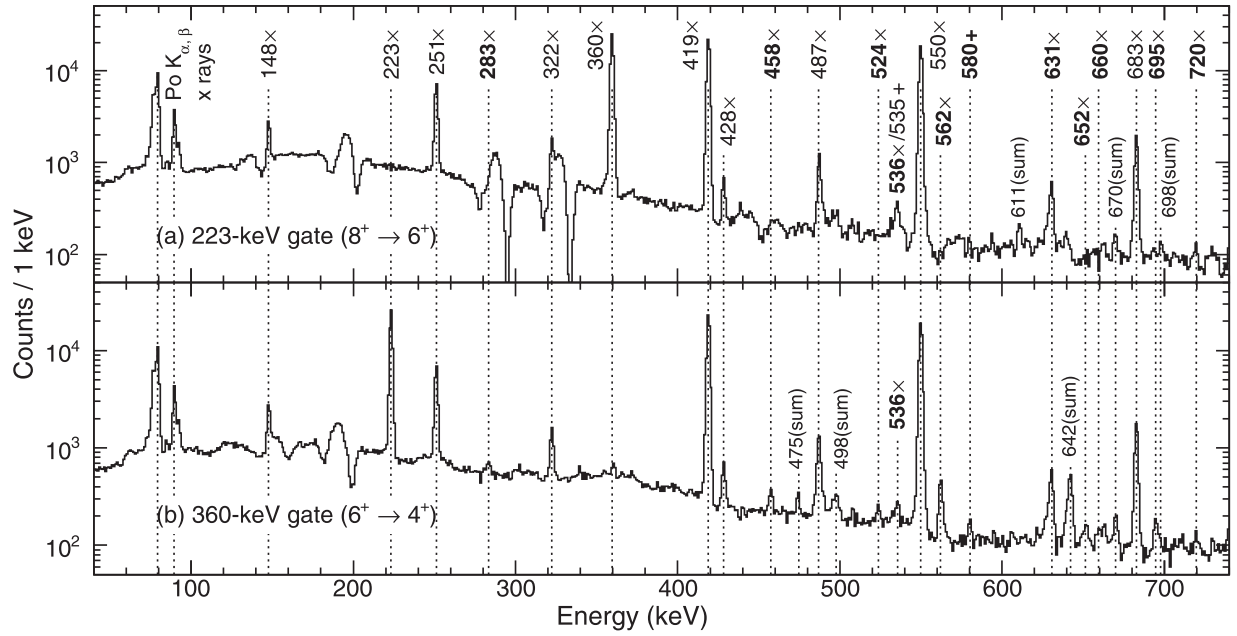


FIG. 3. Lower-energy part of the background-subtracted spectra of  $\gamma$  rays in coincidence with (a) the 223.3-keV ( $8^+ \rightarrow 6^+$ ) and (b) the 359.6-keV ( $6^+ \rightarrow 4^+$ ) transition. The peaks marked with the ( $\times$ ) and ( $+$ ) labels follow the  $\beta^-$  decays of  $^{216}\text{Bi}^g$  and  $^{216}\text{Bi}^m$ , respectively. The 223-keV peak is a doublet, see text for details. The labels written in bold denote new transitions. Peaks marked with “(sum)” are caused by summing transitions in cascades; they are listed in Table II in the Supplemental Material [15]. The broader peak-like structures with depressions in the background around them are artificial peaks caused by Compton scattering.

claimed to be close to 100%, however, the  $\beta$ -particle detection efficiency was not stated.

While gating on the 523.9- or 694.7-keV  $\gamma$  rays, the intensities of the decays from the subsequent cascade (the 359.6-, 418.8-, and 549.8-keV transitions) are higher than the intensity of the 486.1-keV  $\gamma$  ray (spectra of  $\gamma$  rays gated by the relevant transitions are included in Fig. 2 in the Supplemental Material [15]). This could hint that the 486.1-keV transition feeds from the top, and the populated level then decays via parallel 523.9- and 694.7-keV  $\gamma$  rays. However, the total intensity of the 486.1-keV  $\gamma$  ray determined as the difference

in the intensity of the unresolved peak around 487 keV in the singles  $\gamma$ -ray spectrum, containing both contributions to the doublet, and the intensity of the 487.3-keV  $\gamma$  ray determined from the 223.3-keV gate in  $\gamma$ - $\gamma$  coincidences, is 2.2(7) (Table I). This value is higher than the sum of the total 523.9- and 694.7-keV  $\gamma$ -ray intensities of 1.09(5). Therefore, the 523.9- and 694.7-keV  $\gamma$  rays were placed as feeding the 1814.3-keV level, which deexcites via the 486.1-keV transition (Fig. 2). The 523.9-keV  $\gamma$  ray then matches the energy difference between the 2338.2- and 1814.3-keV levels.

The relatively low intensity of the 486.1-keV  $\gamma$  ray compared with subsequent transitions in the gates on the 523.9- and 694.7-keV  $\gamma$  rays can be explained by a high total conversion coefficient. To obtain the same transition intensity for the 486.1-keV decay as for the subsequent yrast band transitions, an  $\alpha_{\text{tot,expt}}(486.1 \text{ keV}) = 1.1(4)$  is needed. The value was obtained as the weighted average of the results of following equation for the two gates in  $\gamma$ - $\gamma$  coincidences:

$$\alpha_{\text{tot,expt}}(486 \text{ keV}) = \frac{\bar{N}_l(\text{subseq.}) - N_\gamma(486 \text{ keV})}{N_\gamma(486 \text{ keV})}, \quad (2)$$

where  $\bar{N}_l(\text{subseq.})$  is the weighted average of counts of the 359.6-, 418.8-, and 549.8-keV transitions obtained using Eq. (1). In this case,  $N_\gamma$  used in Eqs. (1) and (2) is the efficiency-corrected number of counts of the specific  $\gamma$  ray in the respective gates on the 523.9- and 694.7-keV  $\gamma$  rays.

Considering only multiplicities for prompt transitions (up to  $\Delta L = 2$ ), the highest theoretical conversion coefficient for the 486.1-keV transition is only  $\alpha_{\text{tot,th}}(M2) = 0.4$  [32] and thus the experimental value suggests an  $M1 (+E2)$  character

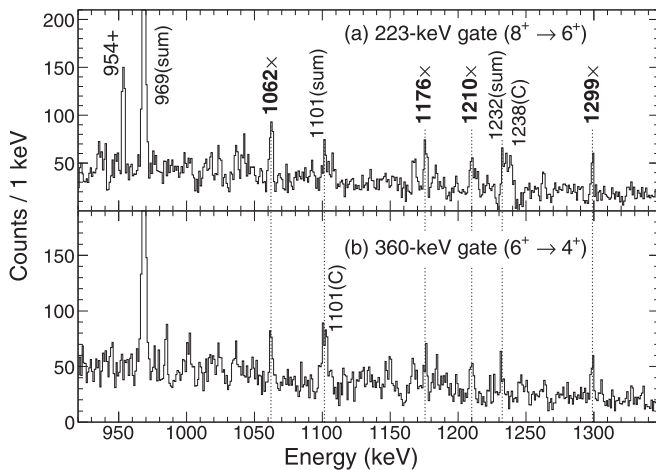


FIG. 4. The same as Fig. 3, but higher-energy part of the spectra. The peaks marked with “C” are caused by the Compton scattering of the 1461-keV line from the decay of  $^{40}\text{K}$ .

TABLE I. A list of  $\gamma$ -ray transitions following the  $\beta^-$  decay of  $^{216}\text{Bi}^g$ .  $E_i$ ,  $E_f$ , and  $E_\gamma$  are the respective energies of the initial and final levels and of the  $\gamma$ -ray transition connecting the levels.  $I_\gamma$  and  $I_t$  are the  $\gamma$ -ray and transition intensities, relative to the intensity of the 359.6-keV  $\gamma$  ray and transition, respectively. Correction for internal conversion needed to calculate  $I_t$  is explained in Sec. III A. Tentative levels or transitions are written in italics. Double dagger ( $\ddagger$ ) marks values, which were deduced from  $\gamma$ - $\gamma$  coincidences.

$E_i$ (keV)	$E_f$ (keV)	$E_\gamma$ (keV)	$I_\gamma$	$I_t$
549.8(2)	0	549.8(2)		
968.6(3)	549.8(2)	418.8(2)		
1328.2(3)	968.6(3)	359.6(2)	100	100
1551.5(4)	1328.2(3)	223.3(2)	74.4(5)	91.5(7)
<i>1611.5(3)</i>	1328.2(3)	283.3(3) $\ddagger$	0.7(2) $\ddagger$	0.8(3) $\ddagger$
	968.6(3)	642.9(2) $\ddagger$	1.0(2) $\ddagger$	1.1(2) $\ddagger$
1699.3(4)	1551.5(4)	147.8(2)	4.05(6)	11(7)
1785.7(4)	1328.2(3)	457.5(2)	0.87(4)	0.88(7)
1802.7(4)	1551.5(4)	251.2(2)	19.07(12)	25(7)
1814.3(4)	1328.2(3)	486.1(3) $\ddagger$	2.2(7) <sup>a</sup>	4.4(16) <sup>a</sup>
1873.9(4)	1551.5(4)	322.4(2)	4.82(6)	5.5(9)
1890.2(4)	1328.2(3)	562.1(2) $\ddagger$	1.5(3) $\ddagger$	1.5(3) $\ddagger$
1979.9(4)	1551.5(4)	428.4(2)	1.91(7)	1.96(17)
	1328.2(3)	<i>651.6(4)<math>\ddagger</math></i>	<i>0.21(11)<math>\ddagger</math></i>	<i>0.21(11)<math>\ddagger</math></i>
2038.8(4)	1551.5(4)	487.3(2) $\ddagger$	4.6(7) $\ddagger$	4.6(8) $\ddagger$
2182.1(5)	1551.5(4)	630.6(2) $\ddagger$	2.5(4) $\ddagger$	2.5(5) $\ddagger$
2234.2(4)	1551.5(4)	682.8(2)	11.62(11)	11.6(8)
2271.1(3)	<i>1611.5(3)</i>	659.6(2) $\ddagger$	0.69(10) $\ddagger$	0.69(11) $\ddagger$
	1551.5(4)	719.8(4) $\ddagger$	0.34(12) $\ddagger$	0.33(12) $\ddagger$
2338.2(4)	1814.3(4)	523.9(2)	0.49(4)	0.48(4)
	1802.7(4)	535.5(3) $\ddagger$	0.54(15) $\ddagger$	0.53(15) $\ddagger$
2508.9(5)	1814.3(4)	694.7(2) $\ddagger$	0.60(3) <sup>b</sup>	0.60(5) <sup>b</sup>
2613.6(5)	1551.5(4)	1062.1(3) $\ddagger$	0.36(12) $\ddagger$	0.35(11) $\ddagger$
2727.5(4)	1551.5(4)	<i>1176.0(3)<math>\ddagger</math></i>	<i>0.47(12)<math>\ddagger</math></i>	<i>0.44(11)<math>\ddagger</math></i>
2761.3(5)	1551.5(4)	1209.8(4) $\ddagger$	0.35(11) $\ddagger$	0.33(11) $\ddagger$
2850.3(5)	1551.5(4)	1298.9(3)	0.29(4)	0.27(4)
		360.4(3) $\ddagger$	0.7(3) $\ddagger$	0.7(3) $\ddagger$

<sup>a</sup>See Sec. III B for details.

<sup>b</sup>Corrected for the contribution from the 695-keV  $\gamma$  ray following the EC/ $\beta^+$  decay of  $^{78}\text{Br}$  [24].

with an  $E0$  component. Such a character would point to an  $I^\pi = (6^+)$  assignment for the 1814.3-keV level.

There is a structure in the decay scheme in Fig. 2 involving the 2271.1- and 1611.5-keV levels and the 283.3-, 642.9-, 659.6-, and 719.8-keV  $\gamma$  rays. Although these de-exciting transitions are present in some of the coincidence spectra in Figs. 3 and 5,  $\gamma$ - $\gamma$  coincidence analysis is hindered by the weak character of the transitions or by overlap with the more intense peaks, such as the 658.5-keV transition attributed to the  $\beta^-$  decay of  $^{216}\text{Bi}^m$  and the 642-keV summing peak (223.3 + 418.8 keV). Thus, the placement in the decay scheme cannot be confirmed by all the relevant gates and is considered as tentative. However, it is supported by the matching energy sums for parallel decay paths within the structure: 283.3(3) + 359.6(2) = 642.9(4) keV is equal to the energy of the crossover 642.9(2)-keV  $\gamma$  ray; 223.3(2) + 719.8(4) = 943.1(5) keV is equal to the sum for the parallel path of 283.3(3) + 659.6(2) = 942.9(4) keV (Fig. 2).

The 642.9-keV transition is placed as feeding the ( $4^+$ ) state, and by itself it would be attributed to the  $\beta^-$  decay of  $^{216}\text{Bi}^m$ . However, the 283.3-keV transition, which deexcites the same 1611.5-keV level as the 642.9-keV decay, feeds the ( $6^+$ ) state. The 2271.1-keV level decays via parallel transitions to the ( $8^+$ ) state and the 1611.5-keV level. Thus, the 642.9-keV  $\gamma$  ray was tentatively attributed to the  $\beta^-$  decay of  $^{216}\text{Bi}^g$ .

In the 359.6-keV gate shown in Fig. 3(b), there is a peak at 360.4(3) keV, which is seemingly a self-coincidence. However, as no such self-coincidences are present in gates on the other intense transitions in Figs. 3(a), 5(a), and 5(b), there is most likely a real 360.4-keV transition above the ( $6^+$ ) level. As it overlaps with much more intense 359.6-keV ( $6^+$ )  $\rightarrow$  ( $4^+$ )  $\gamma$  ray in other coincidence gates, it cannot be placed into the decay scheme, but it can be assigned to the  $\beta^-$  decay of  $^{216}\text{Bi}^g$ .

### C. $\beta^-$ decay of $^{216}\text{Bi}^m$

A similar analysis as for  $^{216}\text{Bi}^g$  was performed also for  $^{216}\text{Bi}^m$ . Coincidences with transitions depopulating two lowest-lying yrast levels, i.e., with the 418.8-keV ( $4^+$ )  $\rightarrow$   $2^+$  and the 549.8-keV  $2^+ \rightarrow 0^+$  transitions, are shown in Figs. 5 and 6 and Fig. 3 in the Supplemental Material [15]. We assigned 66 new transitions and 36 new levels to the  $\beta^-$  decay of  $^{216}\text{Bi}^m$ . The bottom part of the decay scheme and corresponding transitions are presented in Fig. 7 and Table II, the remaining levels and transitions can be found in Figs. 4, 5 and Table IV in the Supplemental Material [15].

The significant extension of the decay scheme was possible because of the orders-of-magnitude higher statistics than in the previous study [5]; for example, the intense 758.6-keV peak contained  $8.7 \times 10^4$  counts in  $\gamma$ -ray singles in the present work (Fig. 1), while in the  $\beta$ -gated  $\gamma$ -ray spectrum in Fig. 7 in Ref. [5] it contained  $\approx 45$  counts. As noted in Sec. III B, the  $\beta$  particle detection efficiency was not stated in Ref. [5].

A systematic shift in  $\gamma$ -ray energies by up to 1 keV between this work and Ref. [5] was observed. However, since the energies were rounded to full keV and no uncertainty was given in Ref. [5], this issue cannot be assessed further.

Despite the high statistics, we could not confirm the 187-, 198-, and 349-keV  $\gamma$  rays visible as weak peaks in Fig. 7 in Ref. [5]. As a result, we removed the 2359-keV state proposed to be depopulated by the latter transition [5]. We note that a 304-keV  $\gamma$  ray and the 304-360-keV coincidence were reported in Ref. [5]. Although we observed a weak 305.2-keV  $\gamma$  ray in  $\gamma$ - $\gamma$  coincidences, gated on the 854.7-keV transition, considering its low intensity (Table II) and position in the decay scheme (Fig. 7), it cannot correspond to the 304-keV  $\gamma$  ray from Ref. [5].

There was a 225-keV  $\gamma$  ray listed in coincidence with the 534-keV transition in Ref. [5], but not placed in the decay scheme. This may correspond to the 223.7-keV transition that we placed as connecting the 1727.1- and 1503.3-keV states shown in Fig. 7. However, we note that a coincidence with the 953.5-keV  $\gamma$  ray depopulating the same 1503.3-keV level,

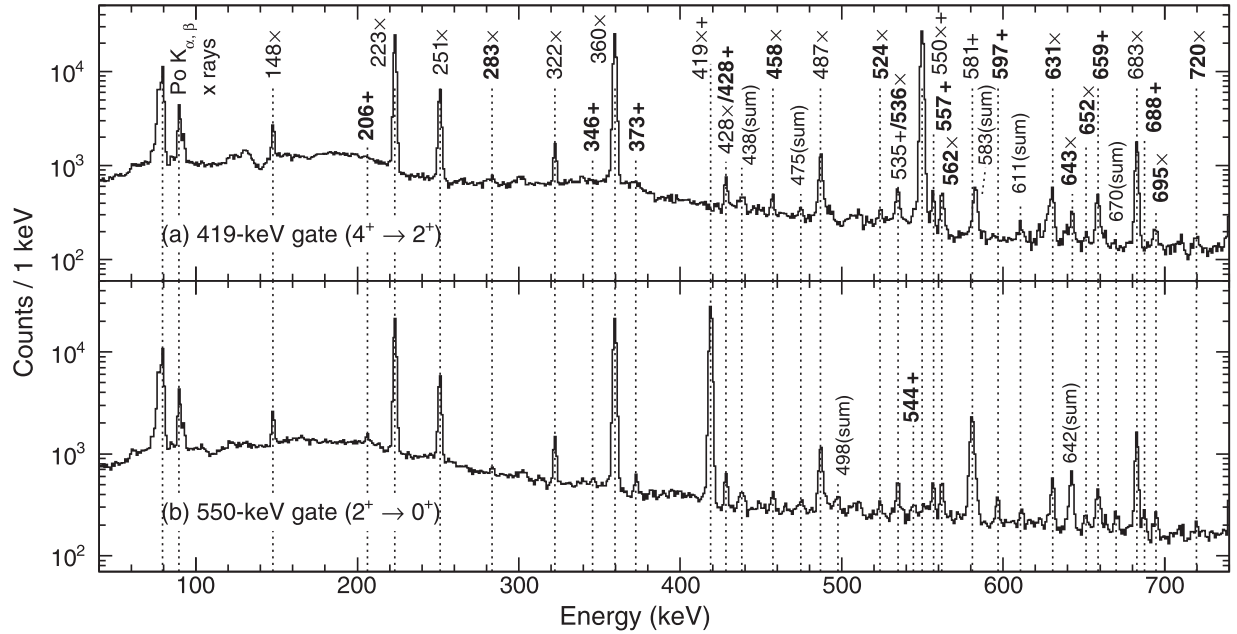


FIG. 5. The low-energy part of the background-subtracted spectra of  $\gamma$  rays in coincidence with (a) the 418.8-keV ( $4^+ \rightarrow 2^+$ ) and (b) the 549.8-keV  $2^+ \rightarrow 0^+$  transition. The peaks marked with ( $\times$ ) and ( $+$ ) labels follow the  $\beta^-$  decays of  $^{216}\text{Bi}^g$  and  $^{216}\text{Bi}^m$ , respectively, transitions with labels in bold are new. Peaks marked with “(sum)” are caused by summing of transitions in cascades, they are listed in Table II in the Supplemental Material [15].

while being much stronger than the 534.9-keV transition (Table II), was not reported in the previous study [5].

Although we confirmed the 581-keV transition [5] (with the energy of 580.9 keV), we moved its position in the decay scheme from feeding the ( $4^+$ ) state to feeding the  $2^+$  state (Fig. 7). The peak close to 580.9 keV in the gate on the 418.8-keV ( $4^+$ )  $\rightarrow$   $2^+$  transition [Fig. 5(a)] has both the energy [582.8(2) keV] and the intensity [ $1.29(20) \times 10^3$  counts]

matching the expected values for the summing peak of transitions in the cascade above the ( $4^+$ ) state (Fig. 2):  $E = 223.3(2) + 359.6(2) = 582.9(3)$  keV and  $N = 1.06(16) \times 10^3$ . The rest of the previously reported decay scheme from Ref. [5] was confirmed.

The numbers of counts of the 549.8- and 418.8-keV transitions, needed to deduce the transition intensities listed in Table II, were corrected for indirect feeding from the  $\beta^-$

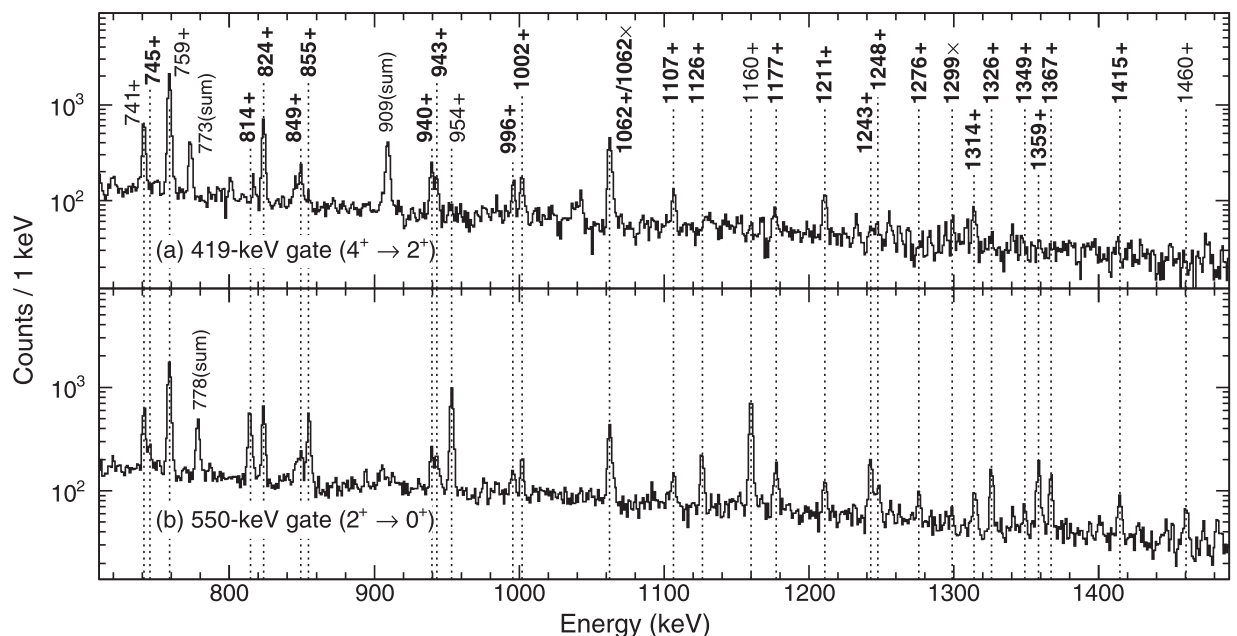


FIG. 6. The same as Fig. 5, but for  $\gamma$  rays between 730–1480 keV.

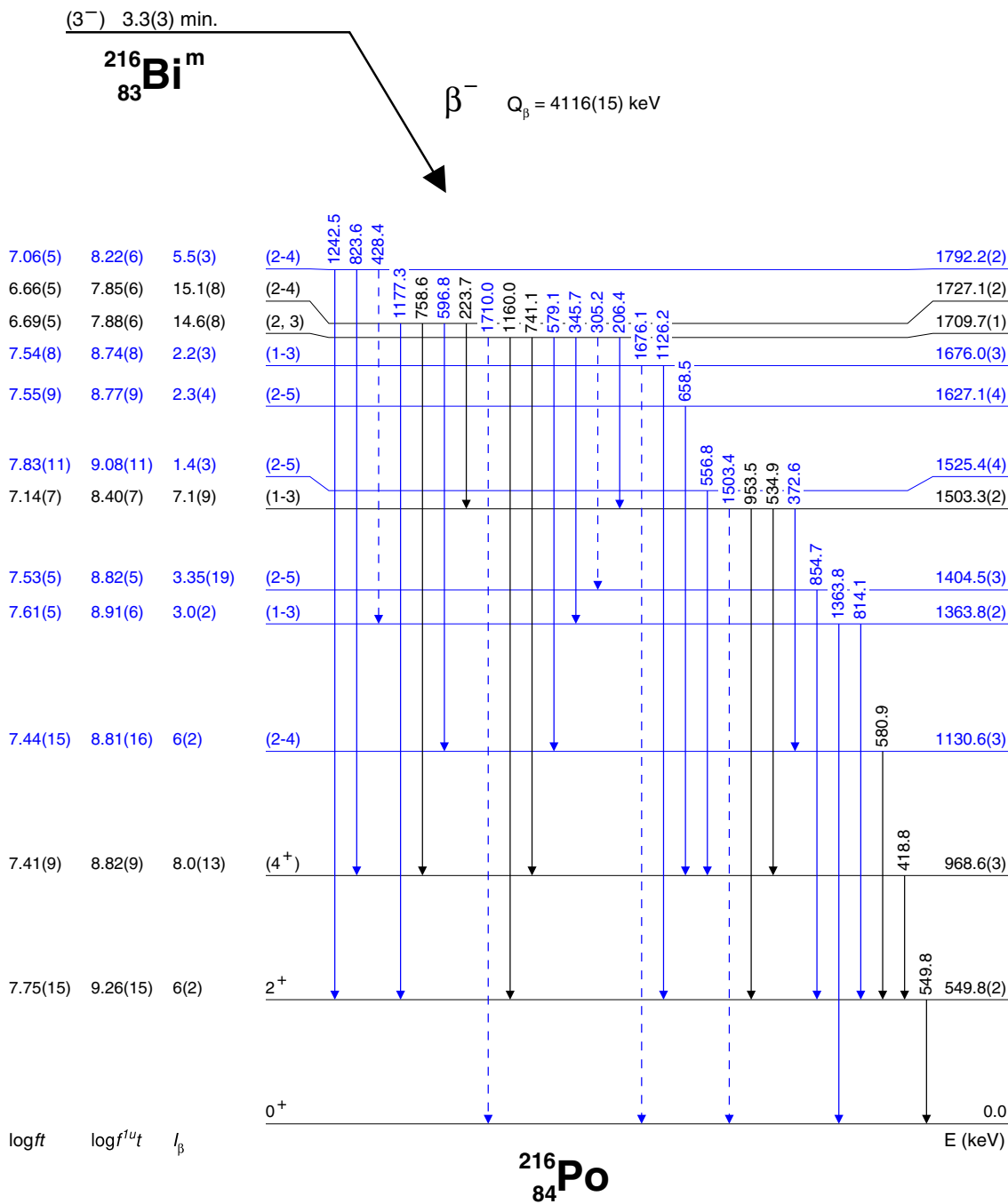


FIG. 7. The first part of the decay scheme with levels in <sup>216</sup>Po populated by the β<sup>-</sup> decay of <sup>216</sup>Bi<sup>m</sup>. The new transitions and levels from the present study are highlighted in blue, while those in black font were reported in Ref. [5]. The half-life of <sup>216</sup>Bi<sup>m</sup>, β-decay feeding intensities and log(ft), log(f<sup>1ut</sup>) values are from this work. All spin and parity assignments are from this work, with an exception of the yrast levels in <sup>216</sup>Po up to the (4<sup>+</sup>) state, which were taken from Ref. [4]. The Q<sub>β</sub> value was calculated as the difference between the atomic mass excesses of <sup>216</sup>Bi<sup>m</sup> and <sup>216</sup>Po taken from NUBASE [10]. For display purposes, the levels up to the 1130.6-keV state are spaced evenly. Dashed lines denote tentative transitions.

decay of <sup>216</sup>Bi<sup>g</sup>, corresponding to the sum of counts of the 359.6- and 642.9-keV transitions feeding the (4<sup>+</sup>) state<sup>1</sup> in

Fig. 2. The corrected numbers of counts of the 549.8- and 418.8-keV transitions were then also converted to numbers of

<sup>1</sup>The number of counts of the 549.8-keV transitions originating from the β<sup>-</sup> decay of <sup>216</sup>Bi<sup>m</sup> is N<sub>t,550 keV</sub>(<sup>216</sup>Bi<sup>m</sup>) = N<sub>t,550 keV</sub> - N<sub>t,360 keV</sub> - N<sub>t,643 keV</sub>, where N<sub>t</sub> values on the right-hand side of the

equation are obtained using Eq. (1). The analogous correction was applied to the 418.8-keV transition.

TABLE II.  $\gamma$ -ray transitions present in the first part of the  $\beta^-$ -decay scheme of  $^{216}\text{Bi}^m$  (Fig. 7). For a detailed explanation of the table, see the caption of Table I. Intensities  $I_\gamma$  and  $I_t$  are relative to the intensity of the 549.8-keV  $\gamma$  ray and transition, respectively. The  $\gamma$ -ray and transition intensities of the 549.8- and 418.8-keV decays were corrected for the indirect feeding from the  $\beta^-$  decay of  $^{216}\text{Bi}^g$ , see Sec. III C for details.

$E_i$ (keV)	$E_f$ (keV)	$E_\gamma$ (keV)	$I_\gamma$	$I_t$
549.8(2)	0	549.8(2)	100	100
968.6(3)	549.8(2)	418.8(2)	43.7(7)	44.7(8)
1130.6(3)	549.8(2)	580.9(2) <sup>‡</sup>	12.2(19) <sup>‡</sup>	12.6(20) <sup>‡</sup>
1363.8(2)	549.8(2)	814.1(2) <sup>‡</sup>	3.06(5)	3.12(14)
	0	1363.8(3) <sup>‡</sup>	2.08(6) <sup>a</sup>	2.05(6) <sup>a</sup>
1404.5(3)	549.8(2)	854.7(2)	3.87(7)	3.93(16)
1503.3(2)	1130.6(3)	372.6(2) <sup>‡</sup>	0.82(12) <sup>‡</sup>	0.91(17) <sup>‡</sup>
	968.6(3)	534.9(3) <sup>‡</sup>	1.33(13)	1.37(15)
	549.8(2)	953.5(2)	7.78(9)	7.81(22)
	0	1503.4(2)	0.20(3)	0.19(3)
1525.4(4)	968.6(3)	556.8(2) <sup>‡</sup>	1.44(25) <sup>‡</sup>	1.5(3) <sup>‡</sup>
1627.1(4)	968.6(3)	658.5(2) <sup>‡</sup>	2.3(4) <sup>‡</sup>	2.4(4) <sup>‡</sup>
1676.0(3)	549.8(2)	1126.2(2) <sup>‡</sup>	1.7(3) <sup>‡</sup>	1.7(3) <sup>‡</sup>
	0	1676.1(2)	0.52(3)	0.51(3)
1709.7(1)	1503.3(2)	206.4(3) <sup>‡</sup>	0.96(23) <sup>‡</sup>	1.6(7) <sup>‡</sup>
	1404.5(3)	305.2(2) <sup>‡</sup>	0.38(7) <sup>‡</sup>	0.47(12) <sup>‡</sup>
	1363.8(2)	345.7(2) <sup>‡</sup>	0.76(11) <sup>‡</sup>	0.88(17) <sup>‡</sup>
	1130.6(3)	579.1(2) <sup>‡</sup>	1.6(3) <sup>‡</sup>	1.7(3) <sup>‡</sup>
	968.6(3)	741.1(2)	3.32(5)	3.43(19)
	549.8(2)	1160.0(2)	7.05(8)	7.00(14)
	0	1710.0(2)	0.13(2)	0.13(2)
1727.1(2)	1503.3(2)	223.7(2) <sup>‡</sup>	0.82(16) <sup>‡</sup>	1.3(5) <sup>‡</sup>
	1130.6(3)	596.8(2)	1.12(6)	1.14(7)
	968.6(3)	758.6(2)	12.23(12)	12.6(6)
	549.8(2)	1177.3(2) <sup>‡</sup>	0.55(22) <sup>‡</sup>	0.54(22) <sup>‡</sup>
1792.2(2)	1363.8(2)	428.4(3) <sup>‡</sup>	0.24(5) <sup>‡</sup>	0.26(6) <sup>‡</sup>
	968.6(3)	823.6(2)	4.02(6)	4.10(17)
	549.8(2)	1242.5(2) <sup>‡</sup>	1.7(3) <sup>‡</sup>	1.7(3) <sup>‡</sup>

<sup>‡</sup>Corrected for the contribution from the 1365-keV  $\gamma$  ray following the  $\beta^-$  decay of  $^{134}\text{Cs}$  [26].

$\gamma$  rays by expressing  $N_\gamma$  from Eq. (1) in order to deduce  $\gamma$ -ray intensities following the  $\beta^-$  decay of  $^{216}\text{Bi}^m$ .

We assigned the 1363.8-, 1503.4-, 1676.1-, 1710.0-, and 1875.9-keV transitions, which are seen in the singles and  $\beta$ -gated  $\gamma$ -ray spectra in Fig. 1, as directly decaying to the g.s. of  $^{216}\text{Po}$  (Fig. 7 and Fig. 4 shown in Supplemental Material [15]). It was possible to confirm the placement of the 1363.8-keV transition by  $\gamma$ - $\gamma$  coincidences, because the respective level is populated by the 345.7-keV  $\gamma$  ray. The remaining four cases were assigned only tentatively based on the matching energy with a level established in  $\gamma$ - $\gamma$  coincidences by a parallel cascade.

A weak 580.2-keV peak was observed in the gate on the 359.6-keV ( $6^+$ )  $\rightarrow$  ( $4^+$ ) transition in Fig. 3(b). It is not possible to set a gate in  $\gamma$ - $\gamma$  coincidences on this 580.2-keV  $\gamma$  ray because it overlaps with much stronger 580.9-keV transition. However, it was tentatively assigned as connecting the 1908.2(2)- and 1328.2-keV levels based on the matching en-

TABLE III. Half-lives deduced from measurement runs for  $^{78}\text{Br}$ ,  $^{216}\text{Bi}^g$ , and  $^{216}\text{Bi}^m$  and their weighted averages ( $A_w$ ). Uncertainties of weighted averages were multiplied by the square root of the reduced  $\chi^2$ .

Run no.	$T_{1/2}(^{78}\text{Br})$ (min.)	$T_{1/2}(^{216}\text{Bi}^g)$ (min.)	$T_{1/2}(^{216}\text{Bi}^m)$ (min.)
130	7.22(79)	2.147(45)	3.70(33)
132	6.08(81)	1.974(37)	3.07(26)
$A_w$	6.7(6)	2.04(9)	3.3(3)

ergy sum: 1328.2(3) + 580.2(3) = 1908.4(5) keV (see Fig. 4 in the Supplemental Material [15]).

It has to be noted, that there are eight levels decaying only to the ( $4^+$ ) state or to structure above this state in the decay scheme of  $^{216}\text{Bi}^m$  (Figs. 4 and 5 in the Supplemental Material [15]). However, considering that the prompt  $\gamma$ -ray transitions may have multipolarities changing spin by two, or even three for higher  $\gamma$ -ray energies, spins of up to  $I = 6$  or even up to  $I = 7$  cannot be ruled out for these eight levels. In the case of such high spins, the levels would in fact have to be fed by the  $\beta^-$  decay of  $^{216}\text{Bi}^g$ . At the same time, for levels with spins  $I = 6, 7$ , a parallel deexcitation path to the ( $6^+$ ) state would be expected and was not observed for the levels in question. To conclude, the assignment of these levels into the  $\beta$ -decay scheme of  $^{216}\text{Bi}^m$  is only tentative but more probable than the possibility that they belong to the decay scheme of  $^{216}\text{Bi}^g$ .

#### D. Half-lives of $^{216}\text{Bi}^g$ and $^{216}\text{Bi}^m$

During the experiment, the beam was continuously implanted on the tape and no dedicated measurement of the decay curves was performed. However, the experiment was divided into several runs, each roughly one hour long, and the tape was moved to remove longer-lived activities before each new run. Therefore, we deduced half-lives of  $^{216}\text{Bi}^{g,m}$  by using the grow-in parts of time distributions in the beginning of the runs. This method relies on the assumption of the constant production rate, which makes it prone to systematic errors because the proton beam intensity was not logged. Moreover, there are additional effects which may influence the grow-in curve or the production rate, such as a change in the distribution of proton pulses within the supercycle, fluctuations of the target temperature, and so on.

To check the stability of the conditions and usability of each run for half-life determination, we also deduced half-life of  $^{78}\text{Br}$ , which was present as a molecular contamination in the beam (Sec. III A and Fig. 1). It has a known half-life of 6.45(4) min. [24], which is of the same order of magnitude as half-lives of  $^{216}\text{Bi}^{g,m}$ . The gate on the 614-keV transition was used to obtain the time distributions for this isotope. Only the runs, where the deduced half-life for  $^{78}\text{Br}$  was consistent with the literature value were considered (Table III).

Additionally, the time distributions for  $^{216}\text{Bi}^g$  were used for selection as well because it had an order-of-magnitude higher statistics than  $^{216}\text{Bi}^m$  or  $^{78}\text{Br}$ , and thus it could also hint at the stability of the measurement. The time distributions for

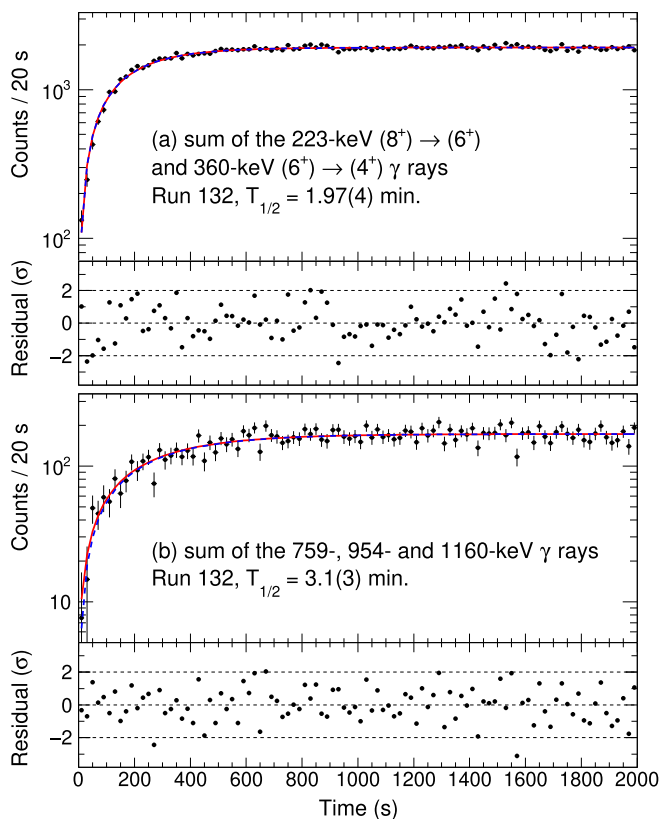


FIG. 8. Background-subtracted time distributions from run 132 for (a) the 223.3- and 359.6-keV  $\gamma$  rays and (b) the 758.6-, 953.5-, and 1160.0-keV  $\gamma$  rays. The line shows the fit to the data. The corresponding normalized residuals of the fits are plotted below each time distribution, dashed lines in these plots mark values of  $-2\sigma$ ,  $0\sigma$ , and  $2\sigma$ .

$^{216}\text{Bi}^g$  were obtained from sums of the gates on the 223.3-keV ( $8^+$ )  $\rightarrow$  ( $6^+$ ) and the 359.6-keV ( $6^+$ )  $\rightarrow$  ( $4^+$ ) transitions. To obtain time distributions for  $^{216}\text{Bi}^m$ , sums of gates on the intense 758.6-, 953.5-, and 1160.0-keV transitions were used. Examples of the time distributions for  $^{216}\text{Bi}^{g,m}$  are shown in Fig. 8 and the half-lives deduced from two runs selected as suitable for half-life determination are listed in Table III. More details on the selection procedure, time distributions from other runs, fitting and deduced values are given in Sec. I in the Supplemental Material [15].

The half-life for  $^{216}\text{Bi}^g$  of 2.04(9) min. is consistent with literature value of 2.22(25) min. [5] and within  $1.3\sigma$  it is also consistent with the value of 2.25(8) min. from Ref. [4]. The half-life for  $^{216}\text{Bi}^m$  of 3.3(3) min. is in agreement with the value of 3.6(4) min. from Ref. [9], while there is seemingly a large discrepancy with the value of 6.6(21) min. reported in Ref. [8]. However, the latter value has a large uncertainty and all three results are consistent within  $1.4\sigma$ .

### E. $\log(ft)$ values

To determine apparent  $\beta$ -decay feeding intensities, the transition intensities were normalized to the number of  $\beta$  decays of the specific state (either  $^{216}\text{Bi}^g$  or  $^{216}\text{Bi}^m$ ). The

apparent  $\beta$ -decay feeding was then deduced as the difference of  $\gamma$ -ray transition intensities per 100 $\beta$  decays feeding and depopulating the specific level.

For  $^{216}\text{Bi}^g$ , the total number of  $\beta$  decays was assumed to be equal to the sum of total intensities of the 359.6-keV ( $6^+$ )  $\rightarrow$  ( $4^+$ ) transition and the 642.9-keV transition bypassing the ( $6^+$ ) state in the  $\beta$ -decay scheme of  $^{216}\text{Bi}^g$  (Fig. 2). Strong  $\beta$ -decay feeding of the ( $8^+$ ) state was observed for  $^{216}\text{Bi}^g$  already in the previous study [4], thus a sizable  $\beta$ -decay feeding of the states with lower spins than  $I = 6$  is unlikely. At the same time, the intensities of the 359.6- and 642.9-keV transitions should not be affected by feeding from the  $\beta^-$  decay of  $^{216}\text{Bi}^m$ ,<sup>2</sup> for which a low spin of  $I = (3)$  was suggested in evaluations [10,14].

For  $^{216}\text{Bi}^m$ , the total number of  $\beta$  decays was estimated as the sum of intensities of transitions feeding the g.s. of  $^{216}\text{Po}$ , that is the sum for the 549.8-, 1363.8-, 1503.4-, 1676.1-, 1710.0-, and 1875.9-keV transitions (see decay schemes in Fig. 7 and Fig. 4 in the Supplemental Material [15]). A direct  $\beta$  decay to the g.s. was considered negligible because of the expected spin of (3) for  $^{216}\text{Bi}^m$  [10,14]. The intensity of the 549.8-keV transition was corrected for indirect feeding by the  $\beta^-$  decay of  $^{216}\text{Bi}^g$ , see Sec. III C for details.

As noted in Sec. III C, there are eight levels in the  $\beta$ -decay scheme of  $^{216}\text{Bi}^m$ , for which it cannot be ruled out that they in fact belong to the  $\beta$ -decay scheme of  $^{216}\text{Bi}^g$ . However, these levels deexcite via relatively weak transitions (see Table IV in the Supplemental Material [15]). Even if they were assigned to the  $\beta^-$  decay of  $^{216}\text{Bi}^g$  and intensities were recalculated according to the modified decay schemes, it would result in a small ( $\approx 9\%$ ) decrease of apparent  $\beta$ -decay feeding intensities for levels in the  $^{216}\text{Bi}^g$   $\beta$ -decay scheme and  $\approx 12\%$  increase for levels in the  $^{216}\text{Bi}^m$   $\beta$ -decay scheme. The relative change in the  $\beta$ -decay intensities is roughly the same for both  $^{216}\text{Bi}^g$  and  $^{216}\text{Bi}^m$ , because the observed  $^{216}\text{Bi}^m$  to  $^{216}\text{Bi}^g$  isomer ratio was 0.96(1). The effect of the change in the intensities on the deduced  $\log(ft)$  values would be negligible.

The  $\log(ft)$  values were deduced using the NNDC  $\log(ft)$  calculator [36]. The  $Q_\beta$  value of 4092(11) keV was taken from AME 2020 [35] and for  $^{216}\text{Bi}^m$ , an excitation energy of 24(19) keV from NUBASE 2020 [10] was used. The  $\beta^-$ -decay branching ratios of both states were assumed to be 100% [14]. For half-lives, our values reported in Sec. III D were taken. Different Fermi integrals, denoted as  $f^{1u}$ , are needed to calculate  $\log(f^{1u}t)$  values for first forbidden unique (FFU)  $\beta$  decays, than those used to calculate  $\log(ft)$  values for allowed (AL) or first forbidden nonunique (FFN)  $\beta$  decays. Therefore, for  $\beta$ -decay feeding of each level,  $\log(ft)$  values, to be compared with systematics for AL and FFN  $\beta$  decays, and  $\log(f^{1u}t)$  values, to be compared with systematics for FFU  $\beta$  decays [37], were calculated. The results are shown in Figs. 2, 7, and Figs. 4, 5 in the Supplemental Material [15].

<sup>2</sup>The possible indirect feeding of the ( $6^+$ ) state by the 580.2-keV transition following the  $\beta^-$  decay of  $^{216}\text{Bi}^m$  was neglected because of its weak intensity and tentative character. The transition is shown in Table IV and Fig. 4 in the Supplemental Material [15].

Although the decay schemes for both states were built up to relatively high excitation energies in  $^{216}\text{Po}$  (2.9 MeV for  $\beta^-$  decay of  $^{216}\text{Bi}^g$  and 3.4 MeV for  $\beta^-$  decay of  $^{216}\text{Bi}^m$ , in comparison to  $Q_\beta \approx 4.1$  MeV [35]), the presence of the pandemonium effect [38] cannot be ruled out. Therefore, the apparent  $\beta$ -decay feedings should be considered as upper limits and the deduced  $\log(ft)$ ,  $\log(f^{1u}t)$  values as lower limits.

#### IV. DISCUSSION

##### A. Spin and parity of $^{216}\text{Bi}^g$

Similarly to the previous study of  $^{216}\text{Bi}^g$  [4], we observed strong apparent  $\beta$ -decay feeding of the  $(8^+)$  level at 1551.5 keV (Fig. 2), resulting in  $\log(ft) = 6.31(17)$ , which is a typical value for AL or FFN decay, while  $\log(f^{1u}t) = 7.54(17)$  is well below the recommended lower limit for FFU decays of  $\log(f^{1u}t) \geq 8.5$  [37]. Considering that only negative-parity states are expected at low excitation energy in  $^{216}\text{Bi}$  (Sec. V A), parity-conserving AL decays can be disregarded. Therefore,  $\log(ft)$ ,  $\log(f^{1u}t)$  values for the  $(8^+)$  level constrain the  $I^\pi$  assignment of  $^{216}\text{Bi}^g$  to  $(7^-, 8^-, 9^-)$ .

Direct feeding of the  $(6^+)$  level at 1328.2 keV was not observed, but considering uncertainties of transition intensities feeding and deexciting the level, an upper limit for the direct feeding of 1.5% was deduced. Therefore, the  $(7^-)$  assignment for  $^{216}\text{Bi}^g$  is unlikely, because both the  $(6^+)$  and  $(8^+)$  levels are yrast states, for which a very similar structure can be expected. The  $I^\pi = (7^-)$  parent state would decay to both of these yrast levels by FFN decays with  $\Delta I = 1$ , thus a comparable  $\beta$ -decay feeding to both of them would be expected.

Taking the upper limit of 1.5% as the feeding of the  $(6^+)$  level, the resulting  $\log(f^{1u}t) \geq 9.0$  value is in the region typical for FFU decays ( $\Delta I = 2$ ). The  $I^\pi$  of  $^{216}\text{Bi}^g$  would be then further constrained to  $(8^-)$ . Considering that the feeding of the  $(6^+)$  level may be weaker or nonexistent, the  $(9^-)$  option (requiring  $\Delta I = 3$  for direct  $\beta$  decay to the  $(6^+)$  level) cannot be fully ruled out. However, the  $(8^-)$  assignment for  $^{216}\text{Bi}^g$  is also supported by SM calculations (Sec. V A).

##### B. Spin and parity of $^{216}\text{Bi}^m$

Two states with at least tentatively known spin and parity, the yrast  $2^+$  and  $(4^+)$  states, are populated in the  $\beta^-$  decay of  $^{216}\text{Bi}^m$ . Apparent  $\beta$ -decay feeding of these two levels is roughly comparable (Fig. 7) and yields  $\log(ft)$  values of 7.75(15) and 7.41(9), respectively, which are consistent with AL or FFN decays. At the same time, both  $\log(f^{1u}t)$  values of 9.26(15) and 8.82(9), respectively, are consistent with FFU decays [37]. Considering that only negative-parity states are expected at low excitation energy in  $^{216}\text{Bi}$  (Sec. V A), the assignment for  $^{216}\text{Bi}^m$  is constrained to  $I^\pi = (2^-, 3^-, 4^-)$ . However, using similar arguments as for  $^{216}\text{Bi}^g$  (Sec. IV A), the most likely assignment is  $I^\pi = (3^-)$ : the  $2^+$  and  $(4^+)$  states are yrast levels with similar structure, thus comparable  $\beta$ -decay feeding suggests the same type of  $\beta$  decay into these states. This condition is fulfilled only for an  $I^\pi = (3^-)$  assignment of the parent state, resulting in FFN decays with  $\Delta I = 1$  to both of the daughter states. This assignment is

consistent with spin (3) suggested in ENSDF evaluation [14] and  $I^\pi = (3^-)$  in NUBASE 2020 evaluation [10].

##### C. Possible second isomer

Reference [5] suggested, that the low-spin, presumably  $(0, 1)$  isomer in  $^{216}\text{Bi}$  was populated in  $\beta^-$  decay of  $0^+$  g.s. in  $^{216}\text{Pb}$ . This was based on the fact, that decays of this state were not observed in direct production in the study [4] at ISOLDE. Although they discussed that the states populated in the  $\beta^-$  decay of  $^{216}\text{Pb}$  would internally deexcite and populate the low-spin isomer in  $^{216}\text{Bi}$ , the  $(3^-)$  state in  $^{216}\text{Bi}$  is treated as another  $\beta$ -decaying state as can be seen in the decay scheme in Fig. 11 in Ref. [5].

However, in our opinion, another low-spin isomer is not necessary to explain the experimental data. If there was a significant indirect production by the  $\beta^-$  decay of  $^{216}\text{Pb}$ , the populated spin 0, 1 states would deexcite to the  $I^\pi = (3^-)$  isomer, unless there was an additional  $0^-$  spin trap. A state with  $I^\pi = 1^-$  is not considered for a possible spin trap, since it would readily deexcite to  $I^\pi = (3^-)$  isomer via an  $E2$  transition. However, such an additional  $0^-$  spin trap is not supported by the SM calculations discussed in Sec. V A, where the  $0^-$  state is predicted a few hundred keV above the  $I^\pi = 1^-, 2^-$  levels. More importantly, the present study was also performed at ISOLDE and we observed the same transitions as Ref. [5] (with the exception of four weak  $\gamma$  rays suggested to belong to  $\beta^-$  decay of  $^{216}\text{Bi}$  in Ref. [5], see Sec. III C). Thus the seeming discrepancy between the two types of experiments disappeared, and it is not necessary to invoke a second isomer.

It is unclear why the levels fed by the  $\beta^-$  decay of  $^{216}\text{Bi}^m$  were not observed in Ref. [4], but it might have been caused by a combination of a few factors. The relative  $\gamma$ -ray intensities reported in Ref. [4] suggest little or no direct  $\beta$ -decay feeding to the  $2^+$  and  $(4^+)$  states, which means a much less favorable isomer ratio for  $^{216}\text{Bi}^m$  than in our study. Even if  $^{216}\text{Bi}^m$  was weakly present in work [4], it would be difficult or impossible to identify it, because its  $\beta$ -decay scheme is fragmented and contains many transitions with relatively low intensities, as was shown in the present high-statistics study. The time structure of the measurement in Ref. [4], consisting of sequences of a 28.8-s-long implantation and 56-s-long beam-off period followed by moving the implantation tape, would also favor shorter-lived  $^{216}\text{Bi}^g$ . If the original isomer ratio in the ion beam was 1 : 1, the observed isomer ratio under such conditions would shift to 1.5 : 1 in favor of  $^{216}\text{Bi}^g$ .

Although both the present work and study [4] were performed at ISOLDE, different proton beam energies, targets, and ionization methods were used: 1-GeV beam,  $^{232}\text{ThC}_2$  target and hot plasma ion source were employed in Ref. [4], while 1.4-GeV beam,  $^{238}\text{UC}_x$  target and laser ionization by RILIS were used in our study. As mentioned in Sec. II, a broad linewidth of the laser was used for the ionization, thus our ionization method is assumed not to be isomer selective. The hot plasma ion source used in Ref. [4] was not isomer selective either. However, different beam energy and target combinations may strongly affect the production of nuclides, as shown for example for francium isotopes [39]. The effects

on production of different isomers in the same isotope are uncertain, but cannot be ruled out. Moreover, higher in-target production of  $^{216}\text{Pb}$ ,  $\beta$ -decaying into low-spin states in  $^{216}\text{Bi}$ , should lead to an increased yield of  $^{216}\text{Bi}^m$ , even if considering that a significant portion of  $^{216}\text{Pb}$  may escape the target before the decay occurs ( $T_{1/2}(^{216}\text{Pb}) \approx 99$  s [40]). Higher yields of neutron-rich lead and bismuth isotopes with increased beam energy are expected based on simulations [41].

#### D. Constraints on spins for levels in $^{216}\text{Po}$ populated in the $\beta^-$ decay of $^{216}\text{Bi}^g$

Apart from the 1328.2-keV ( $6^+$ ) and 1551.5-keV ( $8^+$ ) states with tentative  $I^\pi$  assignments from literature [4], spins and parities of the remaining levels populated in the  $\beta^-$  decay of  $^{216}\text{Bi}^g$  are unknown. Assuming  $I^\pi = (8^-)$  for  $^{216}\text{Bi}^g$  (Secs. IV A and V A), we may constrain the possible spins of the levels based on  $\beta$ -decay feeding intensities and resulting  $\log(ft)$ ,  $\log(f^{1u}t)$  values shown in Fig. 2.

There are three levels, at 1699.3, 1802.7, and 2234.2 keV, with high  $\beta$ -decay feedings of  $I_\beta > 10\%$  and consequently low  $\log(ft)$  values in the range of 6.2–6.6, while  $\log(f^{1u}t)$  values are in the range of 7.1–7.8. These values correspond to AL or FFN  $\beta$  decays and thus limit the spins of the levels to a range of (7–9). Moreover, these levels decay via a single intense transition to the ( $8^+$ ) state (Table I). In the case of  $I = 7$  for an initial state, a relatively intense parallel decay to the ( $6^+$ ) state can be expected. Therefore the possible spins of these three levels are suggested to be  $I = (8, 9)$ .

For the 1611.5-, 1785.7-, and 1890.2-keV levels, FFU  $\beta$  decays cannot be excluded because of  $\log(f^{1u}t)$  values (Fig. 2) above or at the recommended lower limit of  $\geq 8.5$  [37]. However, taking into account the deexcitation paths from these levels, spins of (6, 7) for the former and (6–8) for the two latter states can be tentatively proposed. The same assumption as for conversion coefficient estimates in Sec. III A was used:  $\gamma$ -ray transitions with energies up to 600 keV were assumed to change spin by  $\Delta I \leq 2$ , and transitions with energies above 600 keV were expected to change spin by  $\Delta I \leq 3$ .

The  $\alpha_{\text{tot,expt}} = 1.1(4)$  deduced for the 486.1-keV transition in Sec. III B suggests an  $E0$  component for this decay, which in turn hints at the  $I^\pi = (6^+)$  assignment for the 1814.3-keV level. Although the deduced  $\log(f^{1u}t) = 8.2(2)$  (Fig. 2) is below the recommended lower limit for FFU decays, it is close to it. Even a small unobserved  $\beta$ -decay feeding of  $\approx 0.5\%$  would result in  $\log(f^{1u}t) = 8.27(25)$ , which is consistent with the limit. Moreover, there are a few known exceptions in the systematics, where FFU decays had  $\log(f^{1u}t)$  below the recommended limit [37]. Therefore, we will not draw conclusions from the  $\log(f^{1u}t)$  value for the 1814.3-keV level.

All the remaining levels have  $\log(f^{1u}t) \leq 8.5$  and their spins can be tentatively constrained to  $I = (7-9)$ . States with spins (7–9) can be populated either by AL or FFN decays, therefore the parities were not proposed. However, the spin 6 options can be reached only by FFU decays and would have positive parities.

#### E. Constraints on spins for levels in $^{216}\text{Po}$ populated in the $\beta^-$ decay of $^{216}\text{Bi}^m$

The  $\beta$ -decay feeding pattern of  $^{216}\text{Bi}^m$  (Fig. 7 and Figs. 4 and 5 in the Supplemental Material [15]) is much more fragmented compared with  $^{216}\text{Bi}^g$  (Fig. 2). Nevertheless, in addition to the  $2^+$  and ( $4^+$ ) levels discussed in Sec. IV B, there are five more levels, at 1130.6, 1503.3, 1709.7, 1727.1, and 1792.2 keV, with relatively strong  $\beta$ -decay feeding of  $I_\beta > 5\%$ . The  $\log(ft)$ ,  $\log(f^{1u}t)$  values for the three higher lying levels are consistent with AL or FFN  $\beta$  decays, and assuming  $I^\pi = (3^-)$  for  $^{216}\text{Bi}^m$  (Sec. IV B), we may suggest spins of  $I = (2-4)$  for these levels. Using the same constraint on multiplicities of  $\gamma$ -ray transitions deexciting the level as in Sec. IV D, the spin of the 1709.7-keV state may be limited to  $I = (2, 3)$ . For the 1130.6- and 1503.3-keV states, feeding via FFU  $\beta$  decay cannot be excluded, because  $\log(f^{1u}t)$  values are above or almost at the recommended limit of  $\geq 8.5$  for FFU decays [37]. Their spin assignments will be explained below with the rest of the levels, for which feeding by FFU decays is possible.

All the remaining states (Fig. 7 and Figs. 4 and 5 in the Supplemental Material [15]) are tentatively proposed to have spins of  $I = (2-4)$ , if the respective  $\log(f^{1u}t)$  value was below the limit of  $\geq 8.5$  [37]. In the case the respective  $\log(f^{1u}t)$  value was above or very close to this limit, the possible range of spins is  $I = (1-5)$ . However, FFU decays would feed  $1^+$  states, for which strong  $M1$   $\gamma$ -ray transitions to the g.s. could be expected. If no transition to the g.s. was observed, the spin range for the level was further constrained to  $I = (2-5)$ . Additionally, for the levels at 1130.6, 1363.8, 1503.3, 1525.4, 1676.0, 1875.8, and 1908.2 keV, the possible spins were further limited based on deexciting transitions, in the same way as in Sec. IV D.

Analogously to high-spin states in Sec. IV D, the parities for levels with possible spins reachable by AL or FFN decays, that is spins  $I = (2-4)$ , were not determined. However, spin options 1 and 5 can be reached only by FFU decays and would have positive parities.

### V. COMPARISON WITH THEORY

To discuss the nature of the states in  $^{216}\text{Bi}$  and  $^{216}\text{Po}$ , two SM calculations were carried out by employing two effective interactions: the H208 [42,43] and the well-known modified Kuo-Herling particle interaction (KHPE) [44]. Both calculations were developed for a large valence space composed of the  $0h_{9/2}$ ,  $1f_{7/2}$ ,  $0i_{13/2}$ ,  $1f_{5/2}$ ,  $2p_{3/2}$ ,  $2p_{1/2}$  proton orbitals and the  $1g_{9/2}$ ,  $0i_{11/2}$ ,  $0j_{15/2}$ ,  $2d_{5/2}$ ,  $3s_{1/2}$ ,  $1g_{7/2}$ ,  $2d_{3/2}$  neutron orbitals above the closed core  $^{208}\text{Pb}$ . The single-particle energies for neutrons and protons were based on experimentally known data of  $^{209}\text{Pb}$  and  $^{209}\text{Bi}$  nuclei, respectively [45]. The H208 effective interaction was widely described in Refs. [42,43]. It was successfully used as a reference to interpret several experimental data obtained from the region beyond  $^{208}\text{Pb}$  [3,46,47]. Both the H208 and KHPE interactions were used to describe the new levels identified in  $^{214}\text{Po}$  populated by the  $\beta^-$  decay of isomer in  $^{214}\text{Bi}$  [3] in the same context as in the present work. The full calculations are considered in the studied systems,

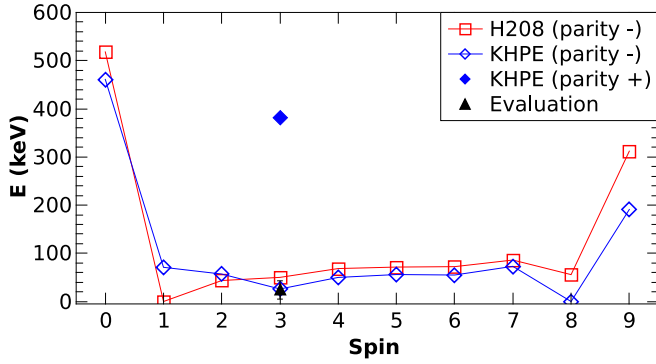


FIG. 9. The calculated energies of low-lying states ( $\lesssim 500$  keV) with spins up to  $I = 9$  in  $^{216}\text{Bi}$  obtained using the KHPE interaction (open blue diamonds for negative-parity states, full blue diamond for positive-parity state) and the H208 interaction (open red squares for negative-parity states). The states stemming from  $\pi 0h_{9/2} \otimes \nu 1g_{9/2}$  multiplet are connected by a line. The black triangle marks the energy of  $I^\pi = (3^-)$  isomer from NUBASE evaluation [10].

and were performed using ANTOINE [48,49] and KSHELL [50] SM codes.

### A. Levels in $^{216}\text{Bi}$

The calculated energies of low-lying states in  $^{216}\text{Bi}$ , along with a point for  $I^\pi = (3^-)$  isomer at 24(19) keV taken from NUBASE 2020 evaluation [10], are displayed in Fig. 9. Most of the yrast states up to the  $9^-$  level, specifically the  $3^- - 6^-$ ,  $8^-$ , and  $9^-$  states, have a dominant  $\pi 0h_{9/2} \otimes \nu 1g_{9/2}$  configuration. Either all seven valence neutrons are occupying the  $\nu 1g_{9/2}$  orbital, or a pair is scattered to higher-lying orbitals, such as  $0i_{11/2}$  or  $0j_{15/2}$ . In addition to the previous configuration, the  $0^- - 2^-$  and  $7^-$  states have strong admixtures. For the  $7^-$  level, the admixture of  $\pi 1f_{7/2} \otimes \nu 1g_{9/2}$  configuration is dominant. The admixtures in the  $0^- - 2^-$  levels are characterized by the occupation of six neutrons in the  $1g_{9/2}$  and one neutron in the  $0i_{11/2}$  orbital, whereas the valence proton occupies the  $0h_{9/2}$  ( $1^-$  level) or  $1f_{7/2}$  orbital ( $0^-$  and  $2^-$  levels).

Both calculations show similar trends and energies (Fig. 9), where all states from  $1^-$  up to  $8^-$  are compressed below 90 keV. In contrast with this, the  $0^-$  and  $9^-$  states are significantly higher in energy, which hints against a long-lived character for these states. The first positive-parity state,  $3^+$ , is also located at a relatively high energy of 381 keV (KHPE) and 797 keV (H208).

Both calculations suggest the existence of two long-lived states, a high-spin state with  $I^\pi = 8^-$  and a low-spin state: in the case of the H208 calculation it has  $I^\pi = 1^-$ , while for the KHPE interaction it has  $I^\pi = 3^-$ . The order of the long-lived states is reversed in the two calculations, KHPE suggests the  $8^-$  state as the g.s., while in the H208 calculation the  $1^-$  level is the g.s.

The  $8^-$  assignment for the high-spin long-lived state is consistent with the  $\beta$ -decay feeding pattern of  $^{216}\text{Bi}^g$  both reported in literature [4] and observed in our study (Sec. IV A).

Therefore, the  $I^\pi = (8^-)$  is proposed as the most likely spin and parity of  $^{216}\text{Bi}^g$ .

The H208 calculation suggests  $I^\pi = 1^-$  for the low-spin long-lived state, which is inconsistent with the observed  $\beta$ -decay feeding pattern (Sec. IV B). However, the energy differences between the levels are very small and even a small change would cause reordering of the levels. Neither of the calculations suggests the existence of a second low-spin long-lived state. Thus, based on the availability of only negative-parity low-lying states and based on the observed  $\beta$ -decay feeding pattern (Sec. IV B),  $I^\pi = (3^-)$  is suggested as the most likely assignment for  $^{216}\text{Bi}^m$ . This assignment is consistent with the KHPE calculation and with evaluations [10,14].

As noted in Sec. I, the order of  $^{216}\text{Bi}^{g,m}$  is not firmly established, because the excitation energy of  $^{216}\text{Bi}^m$  of 24(19) keV from evaluation [10] is low and has a large uncertainty. In Ref. [4],  $^{216}\text{Bi}^g$  was suggested as the g.s. only based on the implications from the parabolic rule [51]. In the present work, this assignment is supported only by one (KHPE) of the two SM calculations. Whether  $^{216}\text{Bi}^g$  is in fact the g.s. remains an open question.

### B. Levels in $^{216}\text{Po}$

Shell-model calculations were also performed for the levels in  $^{216}\text{Po}$  using the two SM approaches introduced in Sec. V. The calculated level energies relevant for the  $\beta^-$  decay of  $^{216}\text{Bi}^g$  are compared with the experimental results in Fig. 10 and an analogous comparison for  $^{216}\text{Bi}^m$  is shown in Fig. 11. The two calculations are mostly in a good agreement with each other, although the levels in KHPE are typically systematically shifted by 100–200 keV to higher energies than the levels in H208. The shift is much more pronounced in the case of  $9^+$  levels, where only the  $9_1^+$  state from KHPE is within the displayed energy range, while there are levels up to the  $9_5^+$  state from H208.

The agreement of the H208 calculation with the experimental yrast  $2^+$  state and presumably yrast ( $4^+$ ), ( $6^+$ ), and ( $8^+$ ) levels is mostly good. However, for KHPE there is again an apparent shift to higher energies for the  $2_1^+$ ,  $4_1^+$ , and  $6_1^+$  states by 100–200 keV compared with the experimental levels. In the H208 calculation, the  $8_2^+$  state is also close in energy to the experimental ( $8^+$ ) level.

The density of nonyrast levels is very high and there are usually at least a few suitable SM states which may correspond to a given experimental level. Therefore we refrain from suggesting any firm assignments. Nevertheless, in the case of high-spin states in Fig. 10, the lowest-lying experimental 1612-keV ( $6, 7$ ) and 1699-keV ( $8, 9$ ) levels might correspond to the SM  $6_2^+$  and  $8_2^+$  states, respectively. The two higher-lying strongly populated states with suggested spins of ( $8, 9$ ) have several candidates for interpretation among the SM  $8^+$ ,  $9^+$  states or even the  $9^-$  level in the case of KHPE. For the states, where suggested spins include  $I = 6$  or  $7$ , there are also SM levels with spins 6 and 7 available.

In contrast with this wider range of spins, to interpret the experimental low-spin states in Fig. 11 there are mostly only SM  $2^+$  and  $4^+$  states available. All the SM states with

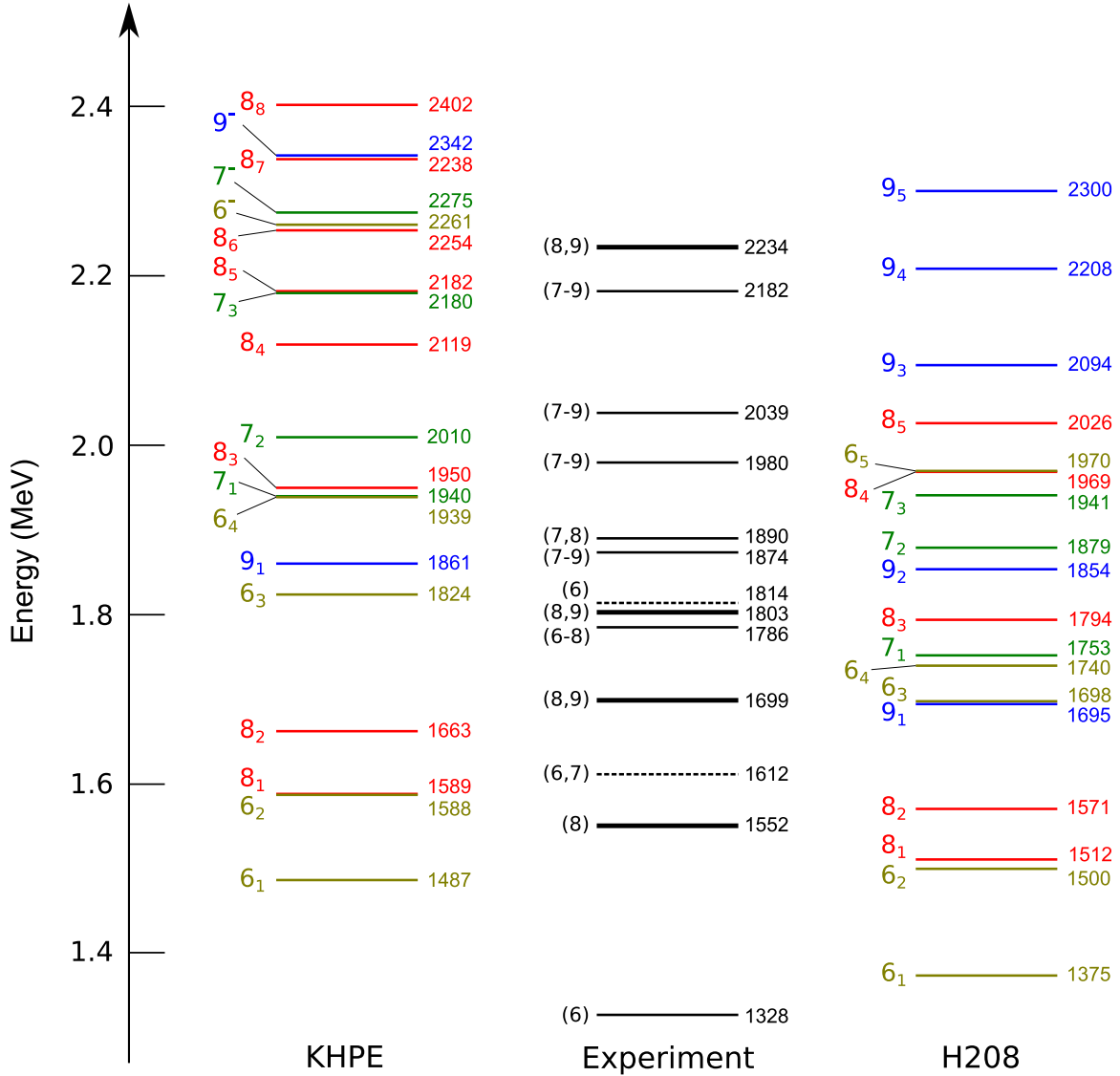


FIG. 10. Comparison of levels in  $^{216}\text{Po}$  from the experiment and from SM calculations based on the KHPE (left) and H208 (right) interactions for the spin range 6–9, relevant for the  $\beta^-$  decay of  $^{216}\text{Bi}^g$ . We note that for the H208 interaction, only five lowest states for a given spin and parity were calculated. Experimental states with strong  $\beta$ -decay feeding ( $I_\beta > 10\%$ ) are highlighted by thicker lines, while only states up to the highest of these strongly fed levels are displayed. All of the SM levels have positive parities, except for the lowest-lying  $6^-$ ,  $7^-$ , and  $9^-$  states from the KPHE calculation at 2261, 2275, and 2342 keV, respectively. Spins are given on the left sides of the levels, energies in keV are given on the right sides. SM levels with the same spins are highlighted in the same colors. Spins of the 1328- and 1552-keV experimental levels were taken from literature [4].

spins of 1, 3, or 5 are predicted above  $\approx 1.69$  MeV. The strongly populated 1131-keV (2–4) level might be then interpreted as the SM  $2_2^+$  state, while the next strongly fed level at 1503 keV with suggested spin of (1–3) could correspond to one of the higher-lying SM  $2^+$  states. However, in the neighboring  $^{214}\text{Bi}$  isotope, the first  $3^-$  state lies already at 1.3 MeV [23]. Therefore, the  $3^-$  option cannot be excluded even for the relatively lower-lying experimental states in Fig. 11. For the strongly populated experimental states

at  $E > 1.7$  MeV, the SM  $2^+$ ,  $3^+$ ,  $3^-$ , and where relevant for the suggested spins ranges, also the SM  $4^+$  levels are available.

The parity of most of the experimental levels discussed in Secs. IV D and IV E could not be deduced. However, almost all available SM states in the displayed energy ranges in Figs. 10 and 11 have positive parities. Therefore, most of the experimental levels included in Figs. 10 and 11 can also be expected to have positive parities.



Two different SM calculations, based on the H208 interaction [42,43] and the modified Kuo-Herling particle interaction (KHPE) [44], were performed for the excited states in  $^{216}\text{Bi}$ ,  $^{216}\text{Po}$  and compared with the experimental results. Both calculations interpret  $^{216}\text{Bi}^g$  as an  $I^\pi = (8^-)$  state, albeit in the KHPE approach it is a ground state, while in the H208 calculation it is an isomer. For  $^{216}\text{Bi}^m$ , its character is interpreted either as an  $I^\pi = (3^-)$  isomer (KHPE) or an  $I^\pi = (1^-)$  ground state (H208), where only the former is consistent with the observed  $\beta$ -decay feeding pattern and the evaluations in literature [10,14].

There is a relatively good agreement between SM calculations and the experiment for the yrast levels up to the presumed  $(8^+)$  state. In the case of nonyrast levels, both the SM calculations and the experimental results show a very high density of states. There are typically several SM states suitable for interpretation for any specific experimental level.

### ACKNOWLEDGMENTS

We acknowledge the support of the ISOLDE Collaboration and technical teams. We are grateful to U. Köster for discussions and advice concerning the origin of the

background and contaminants in the beam. This work has been supported by the Research Foundation Flanders (FWO, Belgium), by BOF KU Leuven (C14/22/104), by GWO and F.R.S.-FNRS under the Excellence of Science (EOS 40007501) programme, by the ENSAR2: European Union's Horizon 2020 research and innovation programme under Grant Agreement No. 654002, by the UK Science and Technology Facilities Council (Grants No. ST/P004598/1 and No. ST/V001027/1), by the Slovak Research and Development Agency (Contracts No. APVV-18-0268 and No. APVV-22-0282), by the Slovak grant agency VEGA (Contract No. 1/0651/21), by the Romanian IFA grant CERN/ISOLDE and Nucleu Project No. PN 23 21 01 02, by Spanish MCIN/AEI/10.13039/501100011033 under Grants No. RTI2018-098868-B-I00, No. PID2019-104390GB-I00, No. PID2019-104714GB-C21, No. PID2021-126998OB-I00 and No. PID2022-140162NB-I00, and by the German BMBF under Grants No. 05P18PKCIA and No. 05P21PKCI1. M.S. acknowledges funding from the European Union's Horizon 2020 research and innovation program under Grant Agreement No. 771036 (ERC CoG MAIDEN) and from the Academy of Finland project No. 354968.

- 
- [1] M. Shamsuzzoha Basunia, *Nucl. Data Sheets* **121**, 561 (2014).  
[2] K. Auranen and E. A. McCutchan, *Nucl. Data Sheets* **168**, 117 (2020).  
[3] B. Andel, P. Van Duppen, A. N. Andreyev, A. Blazhev, H. Grawe, R. Lică, H. Naïdja, M. Stryczyk, A. Algora, S. Antalic *et al.*, *Phys. Rev. C* **104**, 054301 (2021).  
[4] J. Kurpeta, A. Andreyev, J. Äystö, A.-H. Evensen, M. Huhta, M. Huyse, A. Jokinen, M. Karny, E. Kugler, J. Lettry *et al.*, *Eur. Phys. J. A* **7**, 49 (2000).  
[5] A. I. Morales, G. Benzoni, A. Gottardo, J. J. Valiente-Dobón, N. Blasi, A. Bracco, F. Camera, F. C. L. Crespi, A. Corsi, S. Leoni *et al.*, *Phys. Rev. C* **89**, 014324 (2014).  
[6] A. N. Andreyev, A. E. Barzakh, N. Althubiti, B. Andel, S. Antalic, J. Billowes, M. Bissell, K. Chrysalidis, T. E. Cocolios, J. Cubiss *et al.*, <https://cds.cern.ch/record/2241202/files/INTC-P-443-ADD-1.pdf> (2017).  
[7] R. Lică, A. N. Andreyev, L. M. Fraile, N. Mărginean, P. Van Duppen, G. Rainovski, C. Raison, J. Cubiss, M. Monthery, R. Harding *et al.*, <https://cds.cern.ch/record/2288193/files/INTC-P-529.pdf> (2017).  
[8] D. G. Burke, H. Folger, H. Gabelmann, E. Hagebø, P. Hill, P. Hoff, O. Jonsson, N. Kaffrell, W. Kurcewicz, G. Løvholden *et al.*, *Z. Phys. A* **333**, 131 (1989).  
[9] E. Ruchowska, J. Zylicz, C. F. Liang, P. Paris, and C. Briançon, *J. Phys. G* **16**, 255 (1990).  
[10] F. G. Kondev, M. Wang, W. J. Huang, S. Naimi, and G. Audi, *Chin. Phys. C* **45**, 030001 (2021).  
[11] W. J. Huang, M. Wang, F. G. Kondev, G. Audi, and S. Naimi, *Chin. Phys. C* **45**, 030002 (2021).  
[12] L. Chen, W. R. Plaß, H. Geissel, R. Knöbel, C. Kozuharov, Y. Litvinov, Z. Patyk, C. Scheidenberger, K. Siegień-Iwaniuk, B. Sun *et al.*, *Nucl. Phys. A* **882**, 71 (2012).  
[13] C. Weber, G. Audi, D. Beck, K. Blaum, G. Bollen, F. Herfurth, A. Kellerbauer, H.-J. Kluge, D. Lunney, and S. Schwarz, *Nucl. Phys. A* **803**, 1 (2008).  
[14] S.-C. Wu, *Nucl. Data Sheets* **108**, 1057 (2007).  
[15] See Supplemental Material at <http://link.aps.org/supplemental/10.1103/PhysRevC.109.064321> for additional tables and figures.  
[16] R. Catherall, W. Andreatza, M. Breitenfeldt, A. Dorsival, G. J. Focker, T. P. Gharsa, T. J. Giles, J.-L. Grenard, F. Locci, P. Martins *et al.*, *J. Phys. G* **44**, 094002 (2017).  
[17] E. Kugler, *Hyperfine Interact.* **129**, 23 (2000).  
[18] V. Fedosseev, K. Chrysalidis, T. Day Goodacre, B. Marsh, S. Rothe, C. Seiffert, and K. Wendt, *J. Phys. G* **44**, 084006 (2017).  
[19] V. N. Fedoseyev, G. Huber, U. Köster, J. Lettry, V. I. Mishin, H. Ravn, and V. Sebastian, *Hyperfine Interact.* **127**, 409 (2000).  
[20] S. Rothe, T. Day Goodacre, D. V. Fedorov, V. N. Fedosseev, B. A. Marsh, P. L. Molkanov, R. E. Rossel, M. D. Seliverstov, M. Veinhard, and K. D. A. Wendt, *Nucl. Instrum. Methods Phys. Res., Sect. B* **376**, 91 (2016).  
[21] ISOLDE Decay Station; <https://isolde-ids.web.cern.ch/>.  
[22] R. Lică *et al.* (unpublished).  
[23] S. Zhu and E. A. McCutchan, *Nucl. Data Sheets* **175**, 1 (2021).  
[24] A. R. Farhan and B. Singh, *Nucl. Data Sheets* **110**, 1917 (2009).  
[25] Yu. Khazov, A. A. Rodionov, S. Sakharov, and B. Singh, *Nucl. Data Sheets* **104**, 497 (2005).  
[26] A. A. Sonzogni, *Nucl. Data Sheets* **103**, 1 (2004).  
[27] D. Abriola, M. Bostan, S. Erturk, M. Fadil, M. Galan, S. Juutinen, T. Kibédi, F. Kondev, A. Luca, A. Negret *et al.*, *Nucl. Data Sheets* **110**, 2815 (2009).  
[28] Jun Chen, *Nucl. Data Sheets* **146**, 1 (2017).  
[29] Jun Chen, *Nucl. Data Sheets* **140**, 1 (2017).

- [30] M. J. Martin, *Nucl. Data Sheets* **108**, 1583 (2007).
- [31] A. Negret and B. Singh, *Nucl. Data Sheets* **124**, 1 (2015).
- [32] T. Kibédi, T. W. Burrows, M. B. Trzhaskovskaya, P. M. Davidson, and C. W. Nestor, Jr., *Nucl. Instrum. Methods Phys. Res., Sect. A* **589**, 202 (2008).
- [33] R. Nicolini, F. Camera, N. Blasi, S. Brambilla, R. Bassini, C. Boiano, A. Bracco, F. C. L. Crespi, O. Wieland, G. Benzoni *et al.*, *Nucl. Instrum. Methods Phys. Res., Sect. A* **582**, 554 (2007).
- [34] H. De Witte, A. N. Andreyev, I. N. Borzov, E. Caurier, J. Cederkäll, A. De Smet, S. Eeckhaudt, D. V. Fedorov, V. N. Fedosseev, S. Franchoo *et al.*, *Phys. Rev. C* **69**, 044305 (2004).
- [35] M. Wang, W. J. Huang, F. G. Kondev, G. Audi, and S. Naimi, *Chin. Phys. C* **45**, 030003 (2021).
- [36] NNDC  $\log(ft)$  calculator; <https://www.nndc.bnl.gov/logft/>.
- [37] S. Turkat, X. Mougeot, B. Singh, and K. Zuber, *At. Data Nucl. Data Tables* **152**, 101584 (2023).
- [38] J. C. Hardy, L. C. Carraz, B. Jonson, and P. G. Hansen, *Phys. Lett. B* **71**, 307 (1977).
- [39] K. Peräjärvi, J. Cerny, L. M. Fraile, A. Jokinen, A. Kankainen, U. Köster, and J. Äystö, *Eur. Phys. J. A* **21**, 7 (2004).
- [40] R. Caballero-Folch, C. Domingo-Pardo, J. Agramunt, A. Algora, F. Ameil, Y. Ayyad, J. Benlliure, M. Bowry, F. Calviño, D. Cano-Ott *et al.*, *Phys. Rev. C* **95**, 064322 (2017).
- [41] S. Stegemann, J.-L. S. Alvarez, M. Au, E. Aubert, A.-P. Bernardes, C. Bernerd, E. Grenier-Boley, M. Calviani, F. Cerutti *et al.*, <https://cds.cern.ch/record/2809422/files/INTC-P-635.pdf> (2022).
- [42] H. Naïdja, *Phys. Scr.* **94**, 014005 (2019).
- [43] H. Naïdja, *Phys. Rev. C* **103**, 054303 (2021).
- [44] E. K. Warburton and B. A. Brown, *Phys. Rev. C* **43**, 602 (1991).
- [45] J. Chen and F. G. Kondev, *Nucl. Data Sheets* **126**, 373 (2015).
- [46] A. Fernández, A. Jungclaus, P. Golubev, D. Rudolph, L. G. Sarmiento, A. Gargano, H. Naïdja, A. Astier, E. Dupont, A. Gadea *et al.*, *Phys. Rev. C* **104**, 054316 (2021).
- [47] V. Karayonchev, G. Rainovski, J. Jolie, A. Blazhev, A. Dewald, A. Esmaylzadeh, C. Fransen, P. John, L. Knafila, D. Kocheva, K. Schomacker, V. Werner, and H. Naïdja, *Phys. Rev. C* **106**, 064305 (2022).
- [48] E. Caurier and F. Nowacki, *Acta Phys. Pol.* **30**, 705 (1999).
- [49] E. Caurier, G. Martínez-Pinedo, F. Nowack, A. Poves, and A. P. Zuker, *Rev. Mod. Phys.* **77**, 427 (2005).
- [50] N. Shimizu, T. Mizusaki, Y. Utsuno, and Y. Tsunoda, *Comput. Phys. Commun.* **244**, 372 (2019).
- [51] V. Paar, *Nucl. Phys. A* **331**, 16 (1979).